Cat 11

BNWL-1286
UC-80

5-
3-70

[redacted]

METAL SWELLING EFFECTS ON FTR CORE COMPONENTS

March 1970

[redacted]

AEC RESEARCH & DEVELOPMENT REPORT

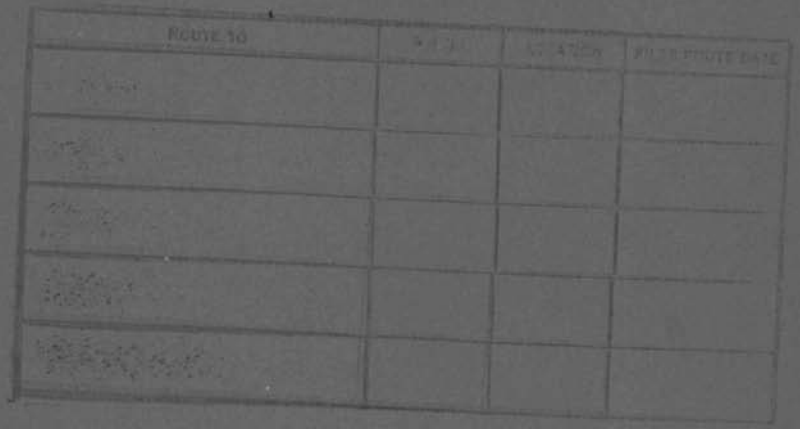

BNWL-1286

BATTELLE NORTHWEST
BATTELLE MEMORIAL INSTITUTE
PACIFIC NORTHWEST LABORATORIES
BATTELLE BOULEVARD, P. O BOX 999, RICHLAND, WASHINGTON 99352

LEGAL NOTICE

This report was prepared as an account of Government sponsored work. Neither the United States, nor the Commission, nor any person acting on behalf of the Commission:

A. Makes any warranty or representation, expressed or implied, with respect to the accuracy, completeness, or usefulness of the information contained in this report, or that the use of any information, apparatus, method, or process disclosed in this report may not infringe privately owned rights; or

B. Assumes any liabilities with respect to the use of, or for damages resulting from the use of any information, apparatus, method, or process disclosed in this report.

As used in the above, "person acting on behalf of the Commission" includes any employee or contractor of the Commission, or employee of such contractor, to the extent that such employee, or contractor of the Commission, or employee of such contractor prepares, disseminates, or provides access to, any information pursuant to his employment or contract with the Commission, or his employment with such contractor.

PACIFIC NORTHWEST LABORATORY
RICHUND, WASHINGTON
operated by
BATTELLE MEMORIAL INSTITUTE
for the
UNITED STATES ATOMIC ENERGY COMMISSION UNDER CONTRACT AT(45-1)-1830

AEC-RL RICHLAND, WASH.

BNWL-1286
UC-80, Reactor Technology

METAL SWELLING EFFECTS ON FTR CORE COMPONENTS

By

R. J. Jackson
C. L. Wheeler
G. R. Waymire
W. W. Little

Reactor and Plant Technology Department
FFTF Division

March 1970

BATTELLE MEMORIAL INSTITUTE
PACIFIC NORTHWEST LABORATORIES
RICHLAND, WASHINGTON 99352

BNWL-1286

Printed in the United States of America
Available from
Clearinghouse for Federal Scientific and Technical Information
National Bureau of Standards, U.S. Department of Commerce
Springfield, Virginia 22151
Price: Printed Copy $3.00; Microfiche $0.65

METAL SWELLING EFFECTS ON FTR CORE COMPONENTS

R. J. Jackson, C. L. Wheeler,
G. R. Waymire, and W. W. Little

ABSTRACT

An elastic analysis which considered neutron-induced metal swelling was performed on each typical component in the Fast Test Reactor (FTR) core. The dilatation and duct bending resulting from the swelling and the swelling gradients are predicted for each component. Component interactions resulting from these dimensional changes are predicted, and duct-to-duct contact between supports during operation is proposed as a potential burnup limitation. Other potential burnup limitations from refueling considerations are discussed.

TABLE OF CONTENTS

LIST OF FIGURES. . . . . .
LIST OF TABLES . . . . . .
INTRODUCTION . . . . . .
SUMMARY. 3
GUIDELINES 5
ENVIRONMENT . . . . . .
Neutron Flux . . . . . .
Wall Temperature 7
Driver Fuel Assemblies 12
Control Rods 14
Closed Loops 18
Reflectors 18
SWELLING DISTRIBUTION 21
Driver Ducts 21
Control Rods 24
Closed Loops 24
INDIVIDUAL COMPONENT SWELLING 25
Driver Ducts 25
Effect of Creep 27
Effect of Temperature on Swelling 27
Control Rods 31
Closed Loops 36
Reflectors 39
INTERACTION OF CORE COMPONENTS DURING OPERATION. . . 41
Interaction Between Driver Ducts 41
Interaction Between Driver Ducts and Control Rods. . 48
Interaction Between Driver Ducts and Closed Loops. . 48
Interaction Between Driver Ducts and Instrument Tree . 48
Interaction Between Driver Duct and Reflectors . . 48
Effect of Creep on Component Interaction 52
Reactivity Change Due to Core Distortion 52

29	Effect of Core Length on Core Deflection	53
30	Effect of Duct Rotation on Displacement	55
31	Predicted 304 Duct Top Deflection Based upon No Component Interaction	58
32	Predicted Duct Top Deflection Based upon No Component Interaction	59

LIST OF TABLES

1	Coefficients of the Control Rod Axial Wall Temperature Functions	18
2	304 Driver Duct Deflection Based upon Elastic Analysis	31
3	316 Driver Duct Deflection Based upon Elastic Analysis	31
4	Predicted Swelling, 316 Cold-Worked Control Rods	34
5	Control Rod Deflection Based upon Elastic Analysis	35
6	Predicted Swelling in 316 Closed Loop Components	38

METAL SWELLING EFFECTS ON FTR CORE COMPONENTS

R. J. Jackson, C. L. Wheeler,
G. R. Waymire, and W. W. Little

INTRODUCTION

The purpose of this study was to develop an understanding of the major interaction between core components of a fast breeder reactor, caused by fast neutron induced metal swelling,[1,2] and to identify the most severe potential problem areas.

---

1. *C. Cawthorne and E. J. Fulton. "Voids in Irradiated Stainless Steel," Nature, vol. 216, p. 575. 1967.*

2. *J. J. Holmes, R. E. Robbins, J. A. Brimhall, and B. Mastel. "Elevated Temperature Irradiation Hardening in Austenitic Stainless Steal," Acta Met. vol. 16, p. 955. 1968.*

SUMMARY

A summary of the results is tabulated below. It may be noted that swelling induced interactions between all major core components are predicted.

Component	Effect of Metal Swelling
General	1. More swelling is predicted for solution-treated 304 than for cold-worked 316 SS.
	2. Lowering the temperature, shortening the core, and rotating the ducts at intervals ameliorate the swelling effects.
Driver Ducts	1. Dilatation is the primary cause of duct to duct contact between Rows 1, 2, and 3.
	2. Duct-bending is largest in Rows 5 and 6.
	3. Based upon elastic stress analysis duct top deflection is almost entirely restrained by the relatively straight reflectors in Rows 7, 8, and 9 during refueling.
	4. Duct-length increase can be accommodated by minor design changes in the instrument tree.
Control Rod	1. Large diametral clearances are required between the guide tube and the inner duct for control rod life greater than six months.
Closed Loops	1. Large volume increases are predicted for the closed loop components, based upon ultimate operating temperatures.
	2. The dilatation and bending associated with the 316 cold-worked closed loops cause duct to duct contact between driver ducts in Rows 5 and the closed loop in Row 6 at about 280 days (~40,000 MWd/tonneM in Row 5 at this time).
	3. A crushing interference between the flow tube and the flow tube liner is predicted because of differential metal swelling of these two coaxial components in the core region.

GUIDELINES

The guide lines used during this study were as follows:

- The FTR design shown in Figure 1 was used as reference.
- The emphasis was on establishing the swelling-induced distorted shape of individual components and then estimating the effects of interactions with other components.
- Thermal stress and distortion were determined to be small in comparison to metal swelling distortion. Only metal swelling was considered for this study.
- The forces between components and the stresses within individual components depend greatly upon the creep rate. Because analytical tools are not presently available to determine the importance of these effects in statically indeterminate beams, no values of force or stress are reported.
- Nominal predicted values for swelling were computed from row-averaged values of temperature and flux. More extreme conditions exist within the core.
- A core lifetime consisting of four 100 day reactor cycles was assumed. This time period causes Row 1 fuel assembly to reach about 100,000 MWd/tonneM peak while the Row 6 fuel assemblies only reach about 50,000 MWd/tonneM burnup at their core midplane. The Row 1 fuel assembly reaches its goal burnup (80,000 MWd/tonneM at about 300 days). The Row 6 fuel assemblies would reach the same goal burnup in about 600 days but would probably reach a burnup limiting distortion earlier. Thus, a 400 day core life with no fuel replacement is a compromise between over-exposure of the center fuel assemblies and under-exposure of the outer fuel assemblies. This compromise permitted a first analysis of the swelling induced core component interactions.

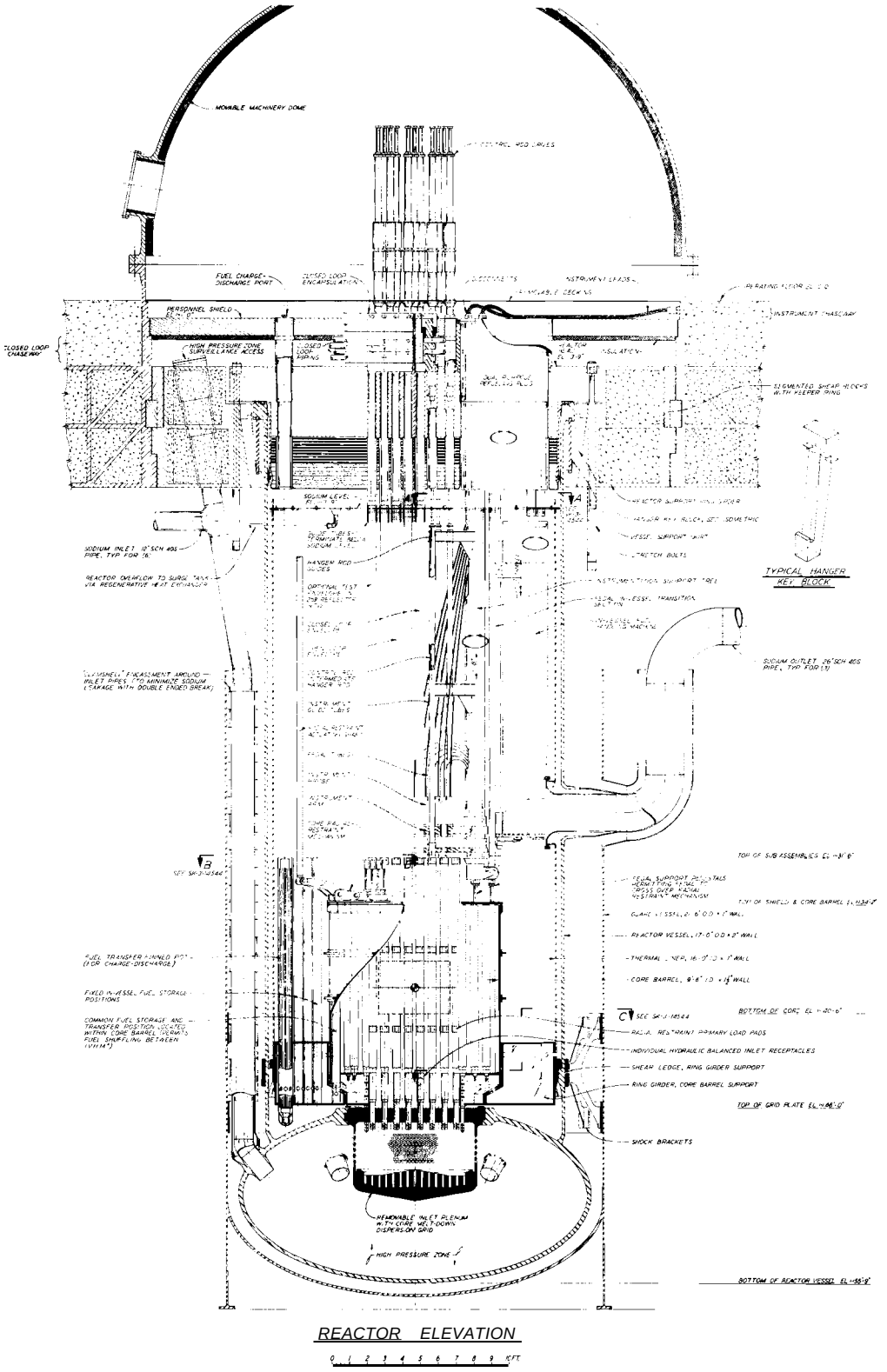

SK-3-14545

FIGURE 1. Reference Reactor Design

ENVIRONMENT

The axial and radial distributions of the neutron flux and metal temperature in the core components are essential to the calculation of their performance.

NEUTRON FLUX

The distribution of total flux is of the form

$$\phi(Z,R,t) = \bar{\phi}\ f(Z)\ g(R,t)$$

where f(Z) is a universal axial profile applicable to all core components, given in Figure 2 along with the functional form used in the swelling analysis. The constants in the assumed functions are determined by a two point fit to previously calculated flux distributions. Figures 3 and 4 illustrate the axial fluence distribution for specified times on the two opposite sides of a Row 6 duct.

The radial profile g(R,t) is given in Figure 5 for the start and end of a typical FTR loading cycle. This profile was obtained from the output of a 2 dimensional diffusion code, 2DB, by averaging the flux over the subassemblies in each row. The time dependence of the radial profile is assumed to vary linearly over each 100 day loading cycle (Figure 6).

The fraction of the total flux with energies greater than 0.1 MeV is assumed to be a constant 65% at all radial locations. This percentage is slightly higher at the interface of the two core zones and slightly lower at the core periphery.

WALL TEMPERATURE

The axial duct wall temperature distribution on the opposite sides of a row averaged duct was calculated for each component.

$$F_Z = 0.570\ e^{0.15Z} \qquad Z < 0$$

$$F_Z = 1.15857\ \text{SIN}\ \frac{(Z + 8.706)}{53.412} \qquad 0 \leq Z \leq 36 \text{ in.}$$

$$F_Z = 0.570\ e^{0.15(36-Z)} \qquad Z > 36 \text{ in.}$$

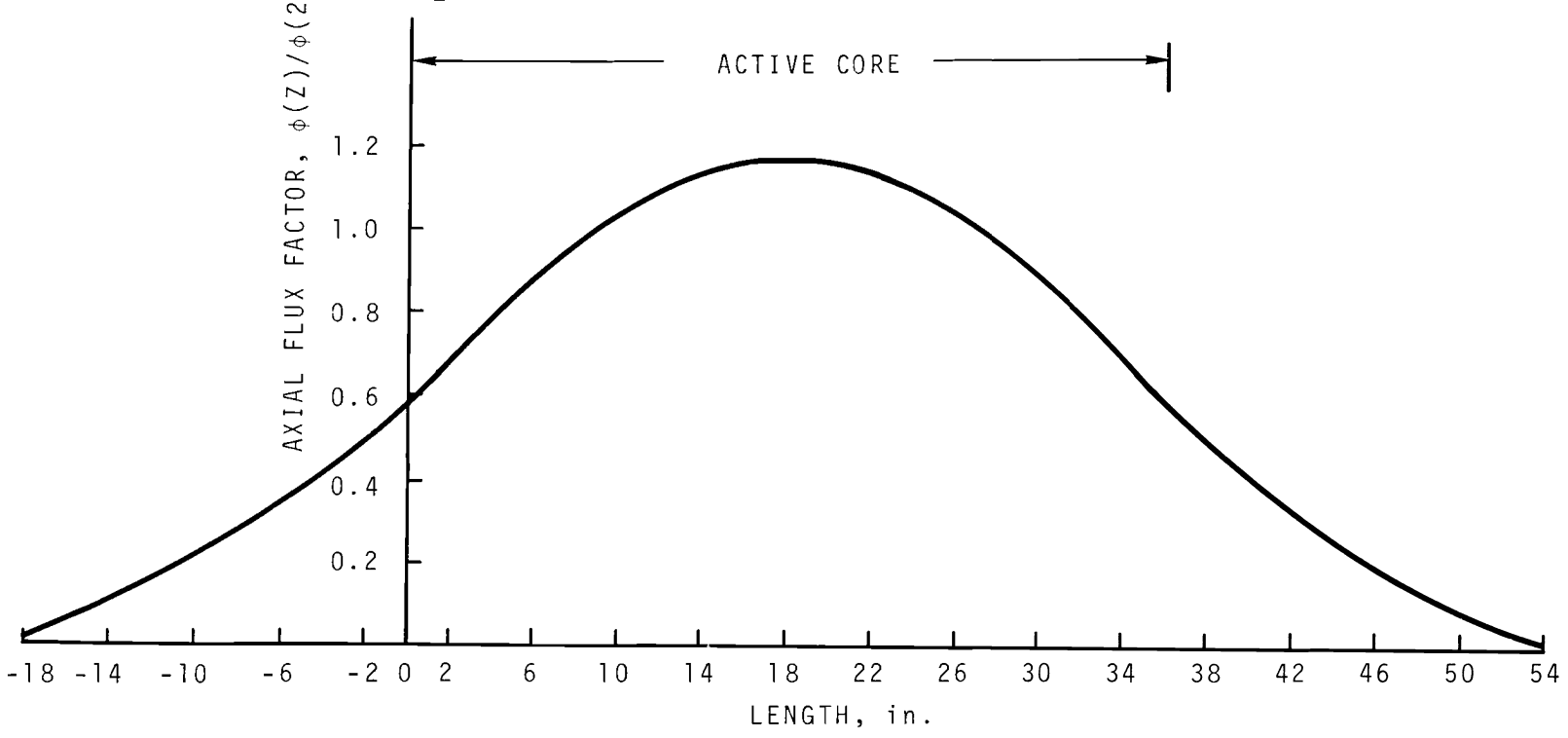

FIGURE 2. Normalized Axial Flux Factor, F_Z

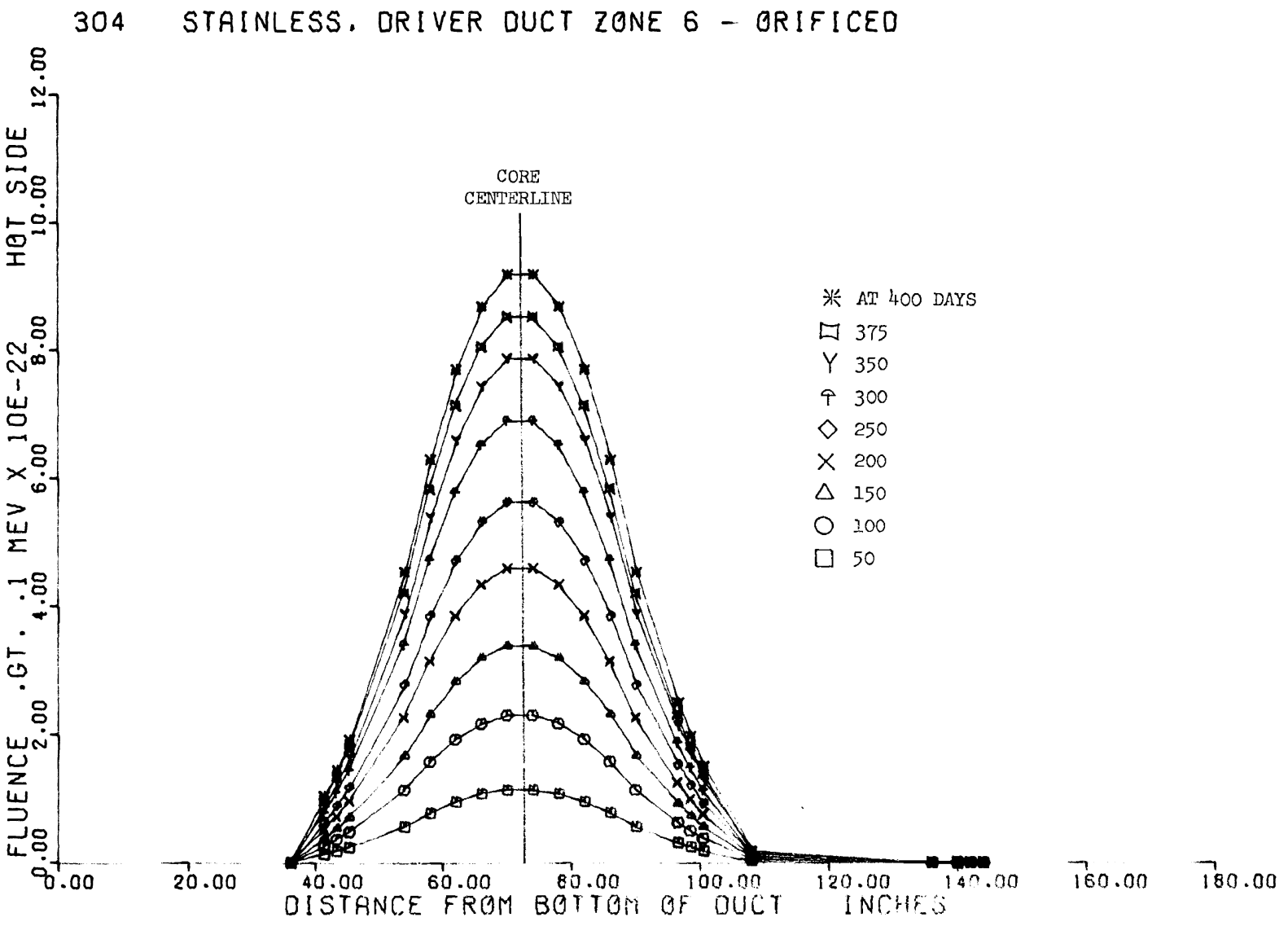

FIGURE 3. Fluence Axial Distribution, Ho ide Row

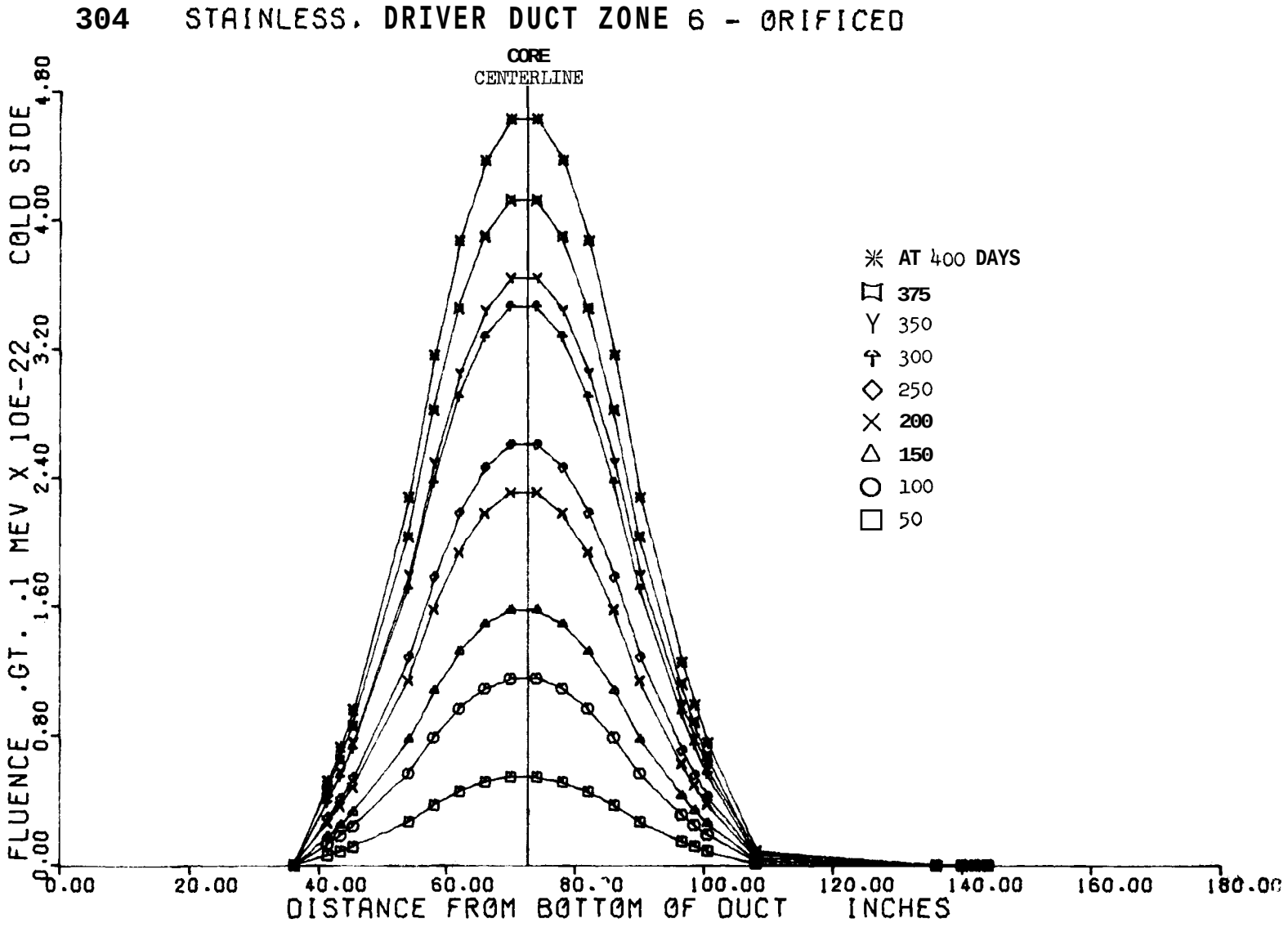

FIGURE 4. Fluence Axial Distribution, Cold Side Row 6

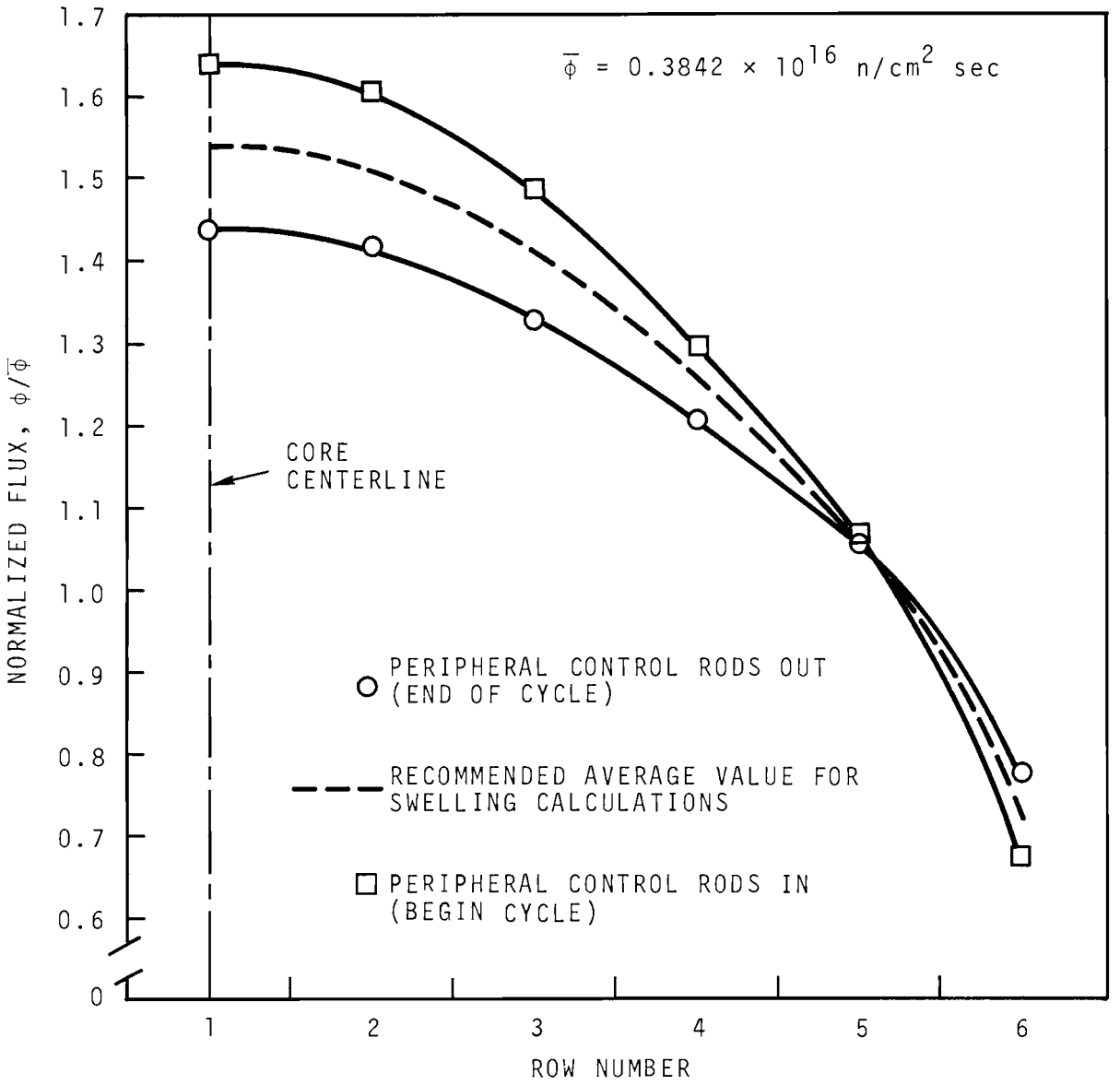

FIGURE 5. Radial Flux Distribution Normalized to 27 in. from Core Bottom

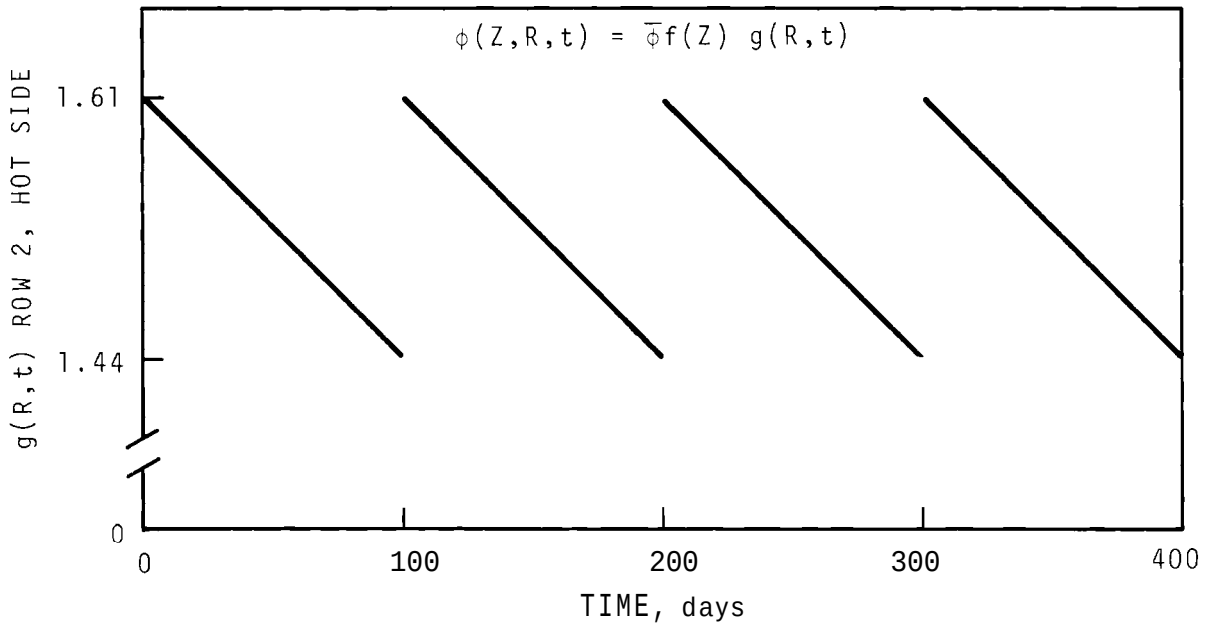

FIGURE 6. Typical Time Dependence of Flux Factor, F_Z

Driver Fuel Assemblies

A linear temperature gradient was assumed between hot and cold sides of the driver ducts. The axial wall temperature profiles were calculated, neglecting heat conduction through the duct wall to the bypass coolant. The bulk temperature of the coolant in the peripheral channels is then used as the duct wall temperature. The coolant temperature profiles are computed by the COBRA Computer code based upon orificed coolant flow rates. The radial power distributions are determined from the same 2DB runs and in the same manner as the radial flux profiles.

Figure 7 presents the row average wall temperatures at 27 in. for the six rows containing driver elements. The functional form of the axial temperature distribution, which fits the computer axial profile, is:

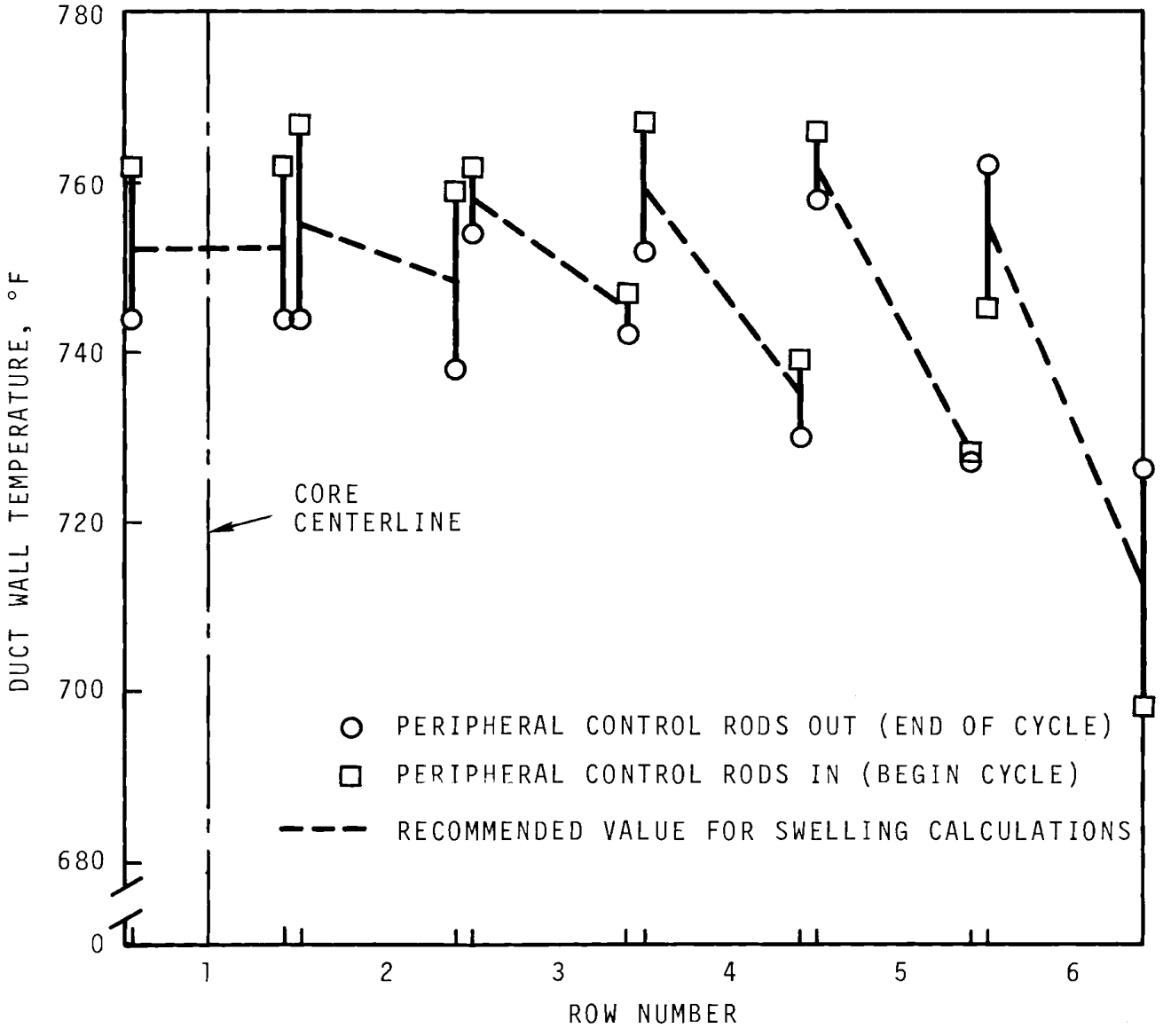

FIGURE 7 Driver Duct Temperatures 27 in rom Core Bottom

$$T(Z) = 600 - [T(27) - 600]\ (0.59478)\left[\frac{\text{Cos}\,\pi\ (Z + 0.75)}{37.5} - 0.99803\right]$$

This expression is used in the computation of temperature for all driver elements. The resultant axial temperature distributions are shown in Figures 8 and 9 for the hot side and cold side of Row 6 respectively.

Control Rods

The coolant temperature in the control rod guide tube prior to its passage through the poison section is the coolant inlet temperature. The small amount of energy carried away by the coolant flowing between the guide tube and inner duct walls is neglected for purposes of calculating duct temperature. Also for this study, the control elements are orificed so that the mean outlet coolant temperature is 800 °F or less. All of the control elements are typified by two types: (1) the in-core control rods located in Rows 4 and 5, and (2) the periphery control rods located in Row 7. The in-core rods are assumed to remain cocked above the core except when the reactor is down. This infers the reactor control is handled completely by the peripheral control rods. We also assumed that these rods move as a bank with a uniform velocity from the fully inserted position at the beginning of each cycle to the fully withdrawn position at the end.

The axial temperature distributions for both the inner and outer walls are given by the following functions.

When:

$$X < X_o$$

$$T - T_o = 0$$

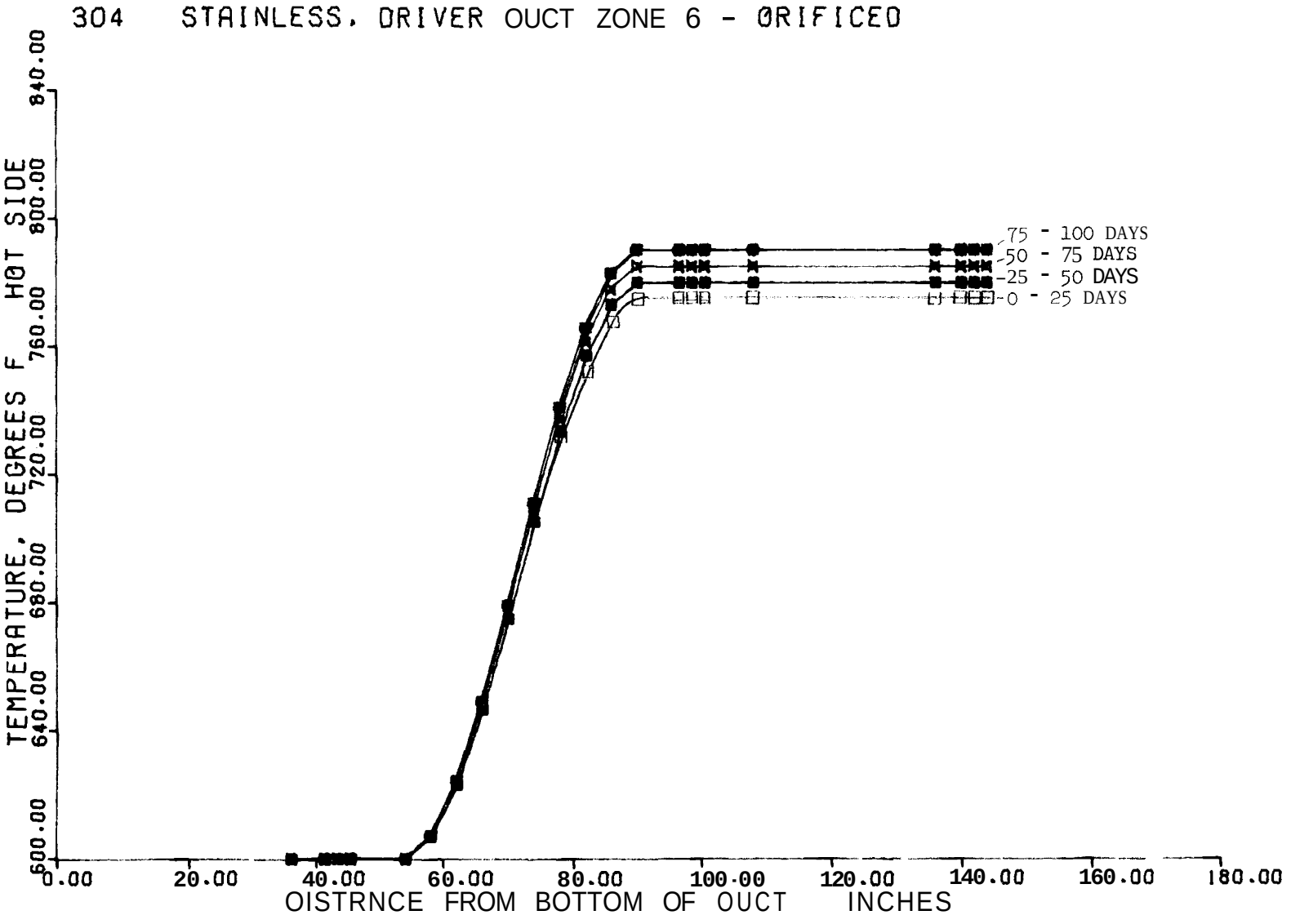

FIGURE 8. Axial Temperature Distribution, Hot Side Row 6

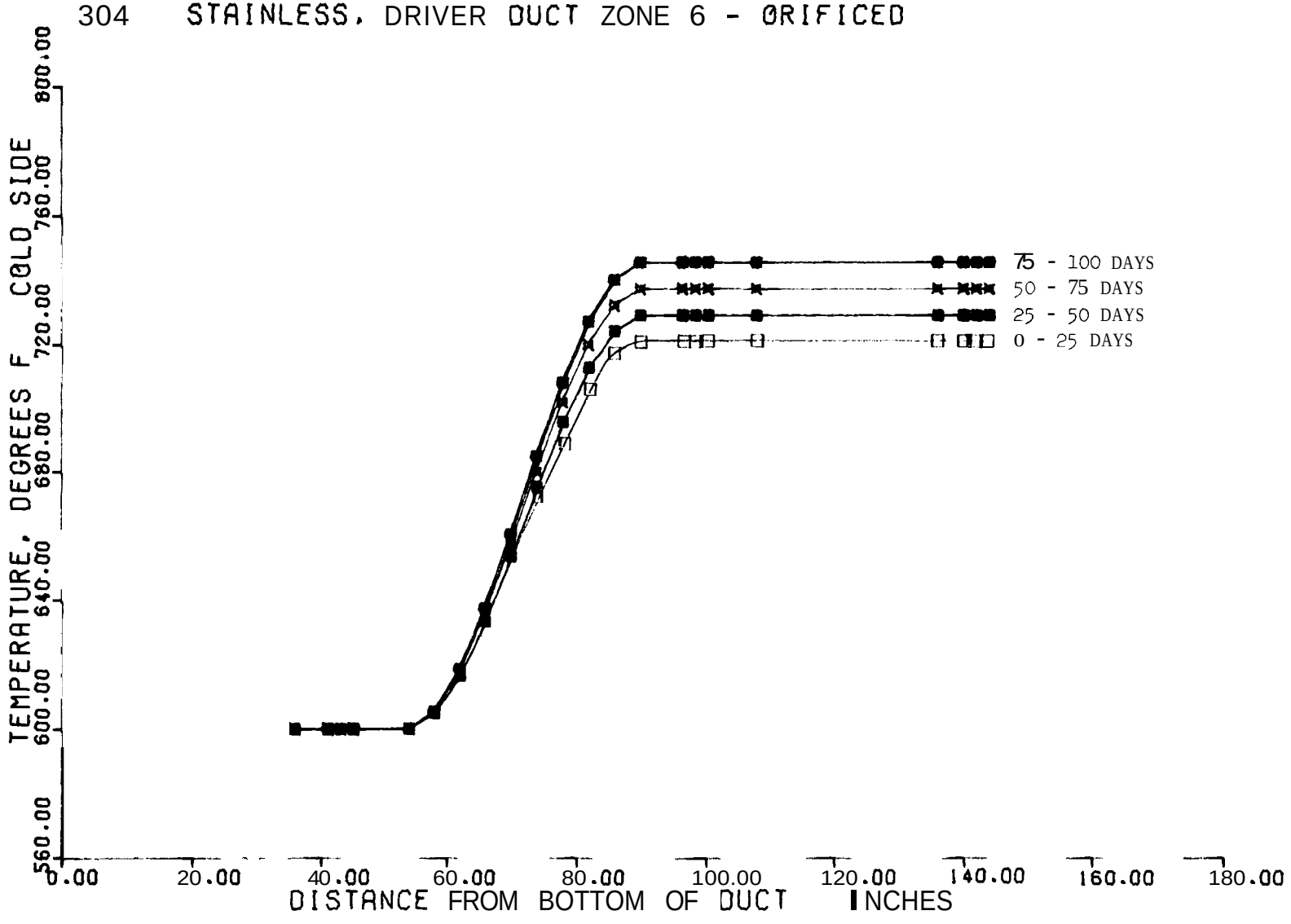

NWL-1286

FIGURE 9. Axial Temperature Distribution, Cold Side Row 6

When:

$$X_o < X < L$$

$$T - T_o = -A\left[\text{Cos}\Pi \frac{X + e}{L + 2e} - \text{Cos}\Pi \frac{X_o + e}{L + 2e}\right]$$

When:

$$X_o < L < X$$

$$T - T_o = -A\left[\text{Cos}\Pi \frac{(L + e)}{L + 2e} - \text{Cos}\Pi \frac{(X_o + e)}{L + 2e}\right] - B\left[e^{-\alpha(X-L)} - 1\right]$$

When:

$$L < X_o < X < X_o + L$$

$$T - T_o = -B\left[e^{-\alpha(X-L)} - e^{-\alpha(X_o-L)}\right]$$

$$L < X_o, \text{ and } X > X_o + L$$

$$T - T_o = -B\left[e^{-\alpha(X_o)} - e^{-\alpha(X_o-L)}\right]$$

Where

T = the temperature at the axial location X, °F

T_o = inlet temperature, taken as 600 °F

X_o = the distance from the bottom of the active core region to the bottom of the active poison element, in.

X = the distance from the bottom of the active core region to the point at which T is computed (may be <0), in.

L = the length of the active core and the length of the poison element, taken as 36 in.

A,e,B,α = constants determined by a curve fit of the data. Numerical values are given in Table 1.

TABLE 1. Coefficients of the Control Rod Axial Wall Temperature Functions

Row	Side	A	e	B	α
4	Hot	65.12	0.75	98.0	0.1268
4	Cold	60.12	0.75	93.0	0.1268
5	Hot	71.64	0.75	108.12	0.1264
5	Cold	58.11	0.75	87.203	0.1192
7	Hot	86.16	0.75	132.49	0.1312
7	Cold	43.58	0.75	65.16	0.1227

Closed Loops

The closed loop wall temperatures were computed by using a finite element computer code for one representative case. The design analyzed consists of two concentric tubes surrounding the test tube. The other two tubes consist of a tube and a liner. The assumed operating conditions are 4.0 MW test with a 1200 °F outlet temperature and 400 °F temperature rise. The computed wall temperatures, as well as the fitted curves used in the swelling calculation, are shown in Figure 10.

Reflectors

The reflectors were assumed to be orificed in such a manner that the bulk mean coolant outlet temperature from each reflector row was 25 °F lower than its inner neighbor. This probable distribution was to prevent thermal shock on the instrument tree components due to high temperature differences between coolant from the driver fuel assemblies and coolant from the shield ducts. The reflector wall temperatures axial distributions were scaled from the driver fuel assembly results. Flux values were obtained from the 2DB runs (discussed under Neutron Flux in the Environment Section).

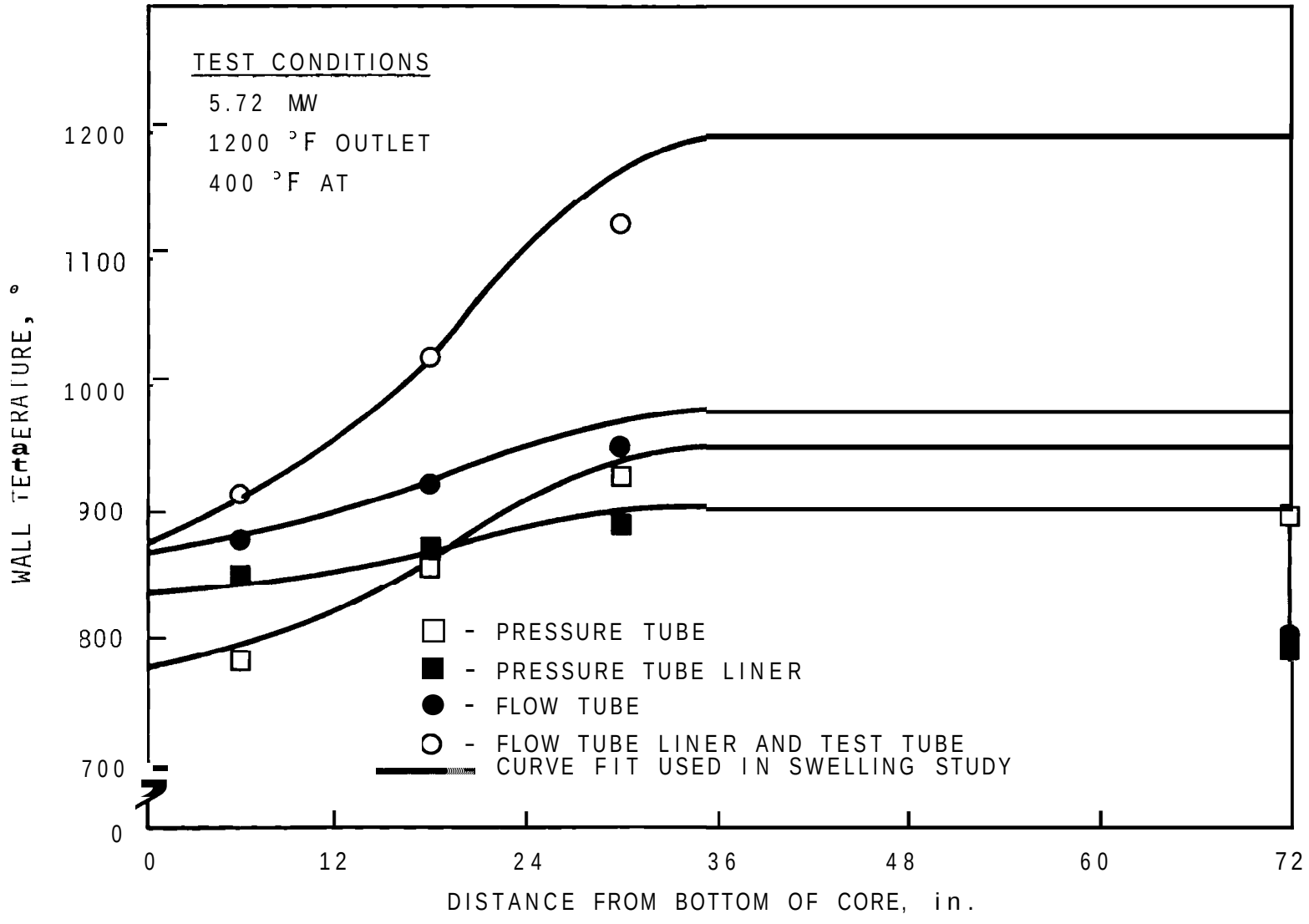

FIGURE 10. Closed Loop Wall Temperatures*

* *Computed* by *D. L. Koreis*

SWELLING DISTRIBUTION

By use of the available swelling data, swelling distributions were calculated for the following components:

Driver fuel assembly ducts	Rows 1 to 6
Control rod	Rows 4, 5, 7
guide tubes	
inner duct	
Closed Loop	Rows 2, 6
pressure tube	
pressure tube liner	
flow tube	
flow tube liner	
test tube	
Reflectors	Rows 7, 8, 9
Shield	Row 10

DRIVER DUCTS

The resulting volume increase in the Row 6 driver ducts is shown in Figures 11 and 12. Note that the peak value of swelling occurs 6 in. above the core midplane. At this elevation after 400-days full-power exposure (approximately 50,000 MWd/tonneM, there is a 4.6% volume increase on the ducts cold side. An average of these two values is used to calculate the increase in dimension across the flats of the duct, with one half of this value reported as the radial dilatation (ΔR). The average swelling value is also used to calculate the increase in duct length (ΔL). The axial swelling distribution of all driver fuel assembly ducts is similar in shape to Figures 11 and 12. After 400 days, the swelling is predicted to be about 10% for solution-treated 304 and about 3 1/2% for cold-worked 316 SS, Row 1, driver ducts.

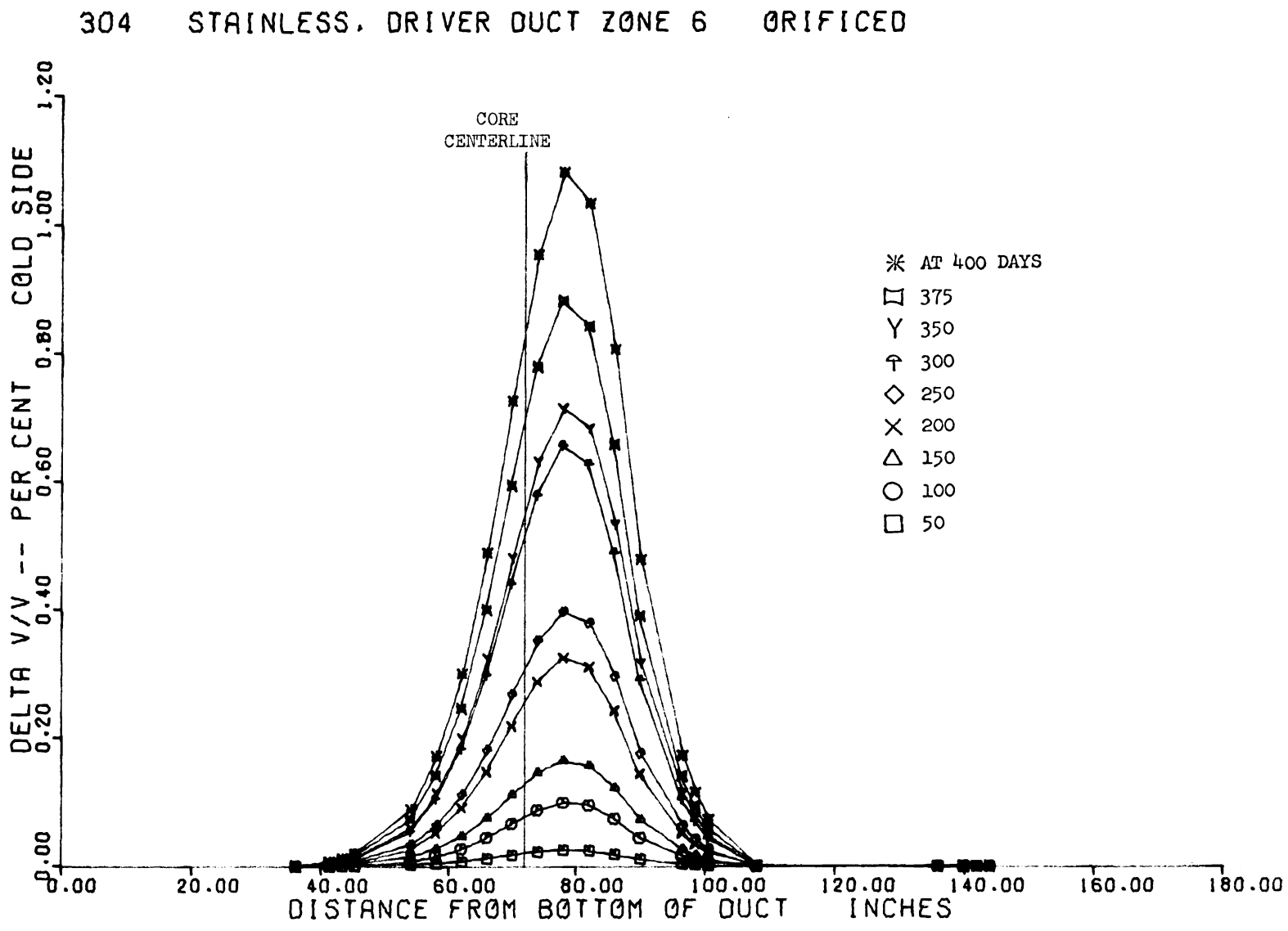

FIGURE 11. Duct Swelling Distribution, Cold Side Row 6

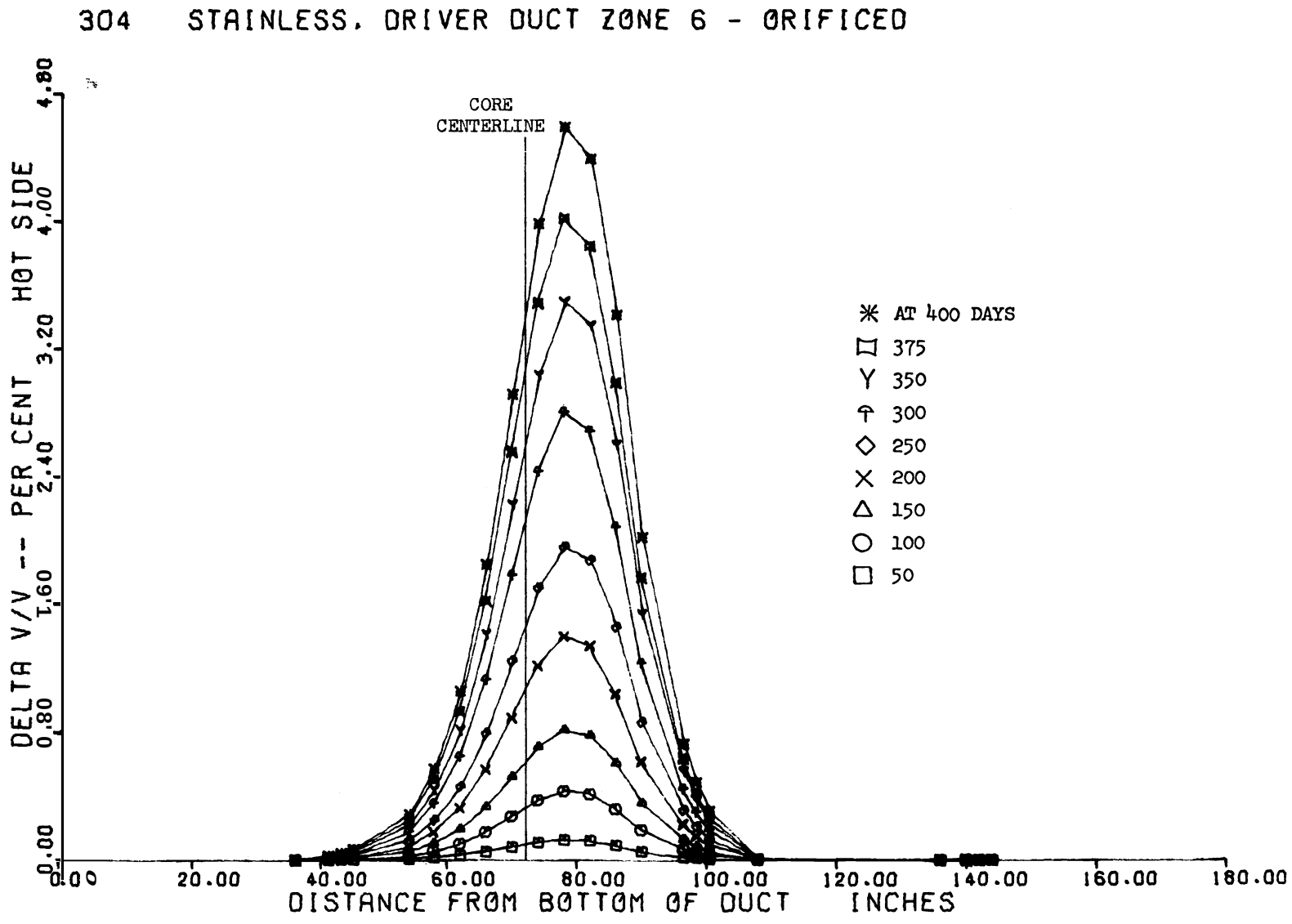

FIGURE 12. Duct Swelling Distribution

CONTROL RODS

The swelling distribution for all control-rod guide tubes and the cocked control-rod inner ducts located in Rows 4 and 5 is similar in shape but lower in magnitude than a driver duct in the same location. The peak occurs at an elevation corresponding to the core midplane. For these components, the maximum calculated swelling is about 2% for solution-treated 304 and about 1 1/2% for cold-worked 316. Because the Row 7 control rod inner ducts are assumed to be shim rods, the swelling distribution is spread along more of their length. The peak swelling value occurs at a point about 4 in. above the bottom of the poison pins. In this component, the maximum calculated swelling is 1 and 1/2% for 304 solution-treated and 316 cold-worked stainless, respectively, after 400 days exposure. For all control rod components, the increase of dimension with time increases monatonically similar to Figure 12.

CLOSED LOOPS

Large values of swelling were calculated for the closed loop components having the same axial distribution shape as for the driver fuel assembly ducts. These larger values result from the high metal temperature in the closed loop components. In Row 2, after 400 days, the maximum swelling was predicted to be about 20% in 304 solution-treated and to vary from 6 to 12% in the different closed loop components for cold-worked 316 stainless ducts. This variation in the predicted 316 swelling is a result of the increased sensitivity to temperature of cold-worked 316 stainless in the operating range of the closed loops. Somewhat similarly, in Row 6, the predicted swelling for 304 solution-treated closed loop components at 400 days is about 8% and is from 2 to 4% in 316 cold-worked components.

INDIVIDUAL COMPONENT SWELLING

The impact of swelling upon the FTR core performance results from axial length increase ($\Delta\ell$), radial dilatation (ΔR), and radial motion of the fuel (6). The radial motion of the fuel is caused by inward duct bending (toward the core center) in the absence of creep. The inward bow is caused by the difference in swelling between two opposite sides of the duct. Average swelling values are used to predict the radial dilatation and the axial length increase of core components. The radial dilatation is reported as one half the increase in dimension across the flats. The magnitude of this swelling are discussed in this section, while the effect of these distortions will be discussed in the next section (Interaction of Core Components During Operation).

DRIVER DUCTS

The predicted radial dilatation from metal swelling is graphically shown in Figure 13. Similar relationships are applicable for 316 cold-worked material.

Because the reference nominal clearance between FTR ducts is 0.100 in., contact between adjacent straight ducts is expected when each has experienced 0.050 in. radial dilatation. Examination of Figure 13 (304 SS) indicates that Rows 1 and 2 will contact after about 300 days exposure. This is erroneous because an elastic analysis indicates that Row 2 duct bends inward from differential swelling instead of remaining straight and contact will occur sooner than 300 days because of this duct bending.

Duct bending is calculated by first deternining the moment that would cause the same curvature of an unrestrained duct as is caused by the difference in swelling on the two opposite sides of the duct. This moment is considered to be the applied moment to the restrained duct. Applied moments for a Row 6

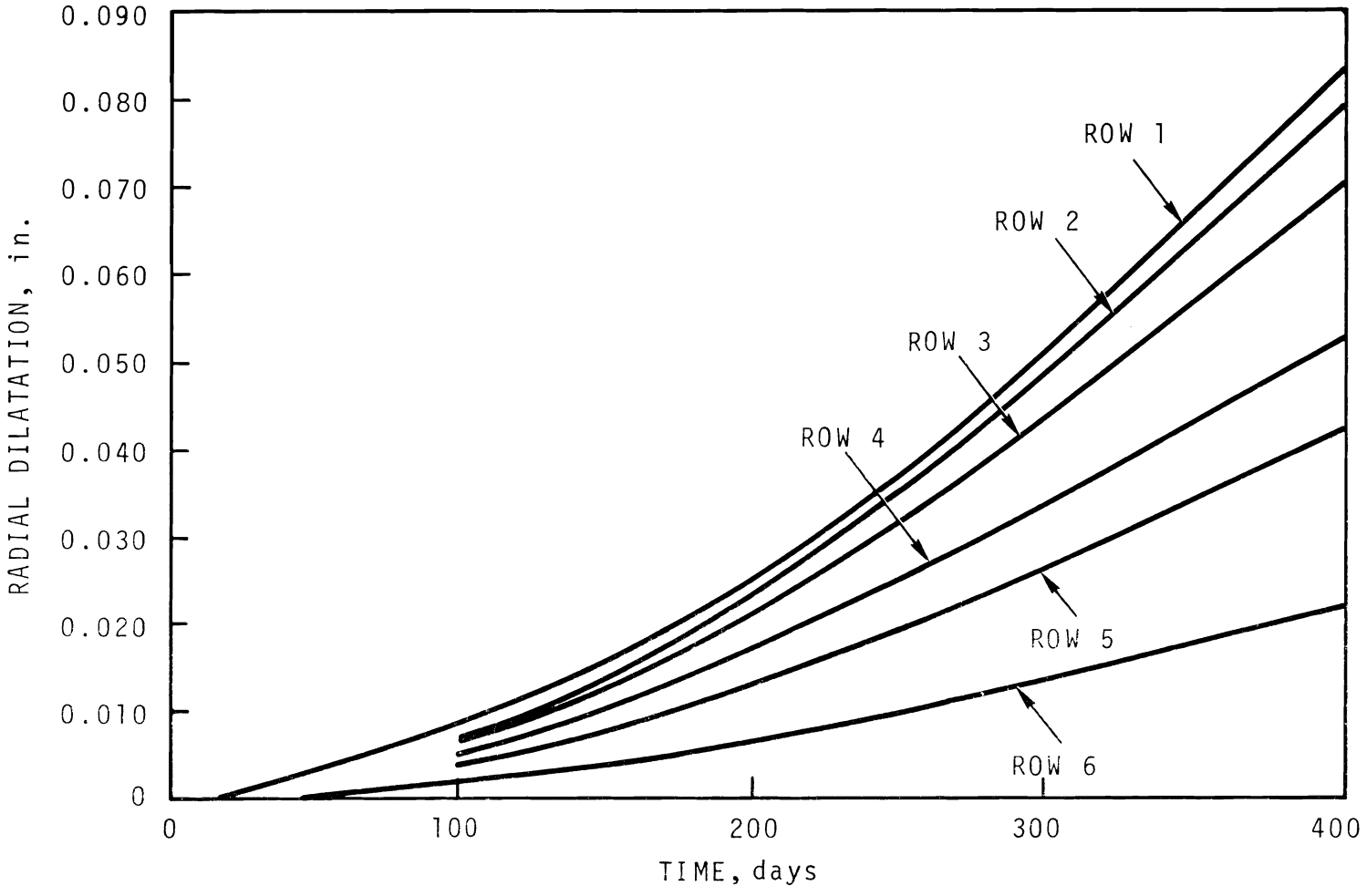

FIGURE 13 Radial Dilatation of 304 Driver Ducts, at 6 in. Above Core Midplane

driver duct are shown in Figure 14. The resulting deflections are then calculated with the MIT STRESS computer code which uses elastic theory. Figure 15 displays the deflection results for a duct after 200 days exposure which was supported as indicated in Figure 16. Note that the maximum deflection occurs in the core region about 6 in. above the core midplane--the same elevation where the maximum swelling and the maximum applied moment occurs. Corresponding maximum in-core deflections for the other rows of ducts are tabulated in Tables 2 and 3 for solution-treated 304 and cold-worked 316, respectively. Figure 17 illustrates the relationship between these predicted core deflections for the various driver ducts as a function of time. Note that Row 6 has the highest deflection values.

Effect of Creep

The duct top deflection during refueling is caused by the nonrecoverable deformation of differential swelling and the elastic recovery of bending stress. Any creep strain occuring during operation will reduce the elastic recovery of bending stress and will, thereby, reduce the amount of duct top deflection. The duct wall temperatures are too low for thermally activated creep mechanisms to be effective. However, crude calculations indicate that the amount of in-reactor creep at these low temperatures is still sufficient to reduce the duct top deflection substantially (by a factor presently believed greater than 2). Computer codes are required to study this in detail.

Effect of Temperature on Swelling

Figure 18 indicates a significant reduction of swelling occurs for a relatively minor temperature decrease. For example, if the metal temperature at the core top were reduced 50 °F below the value for the reference FTR core (somewhat

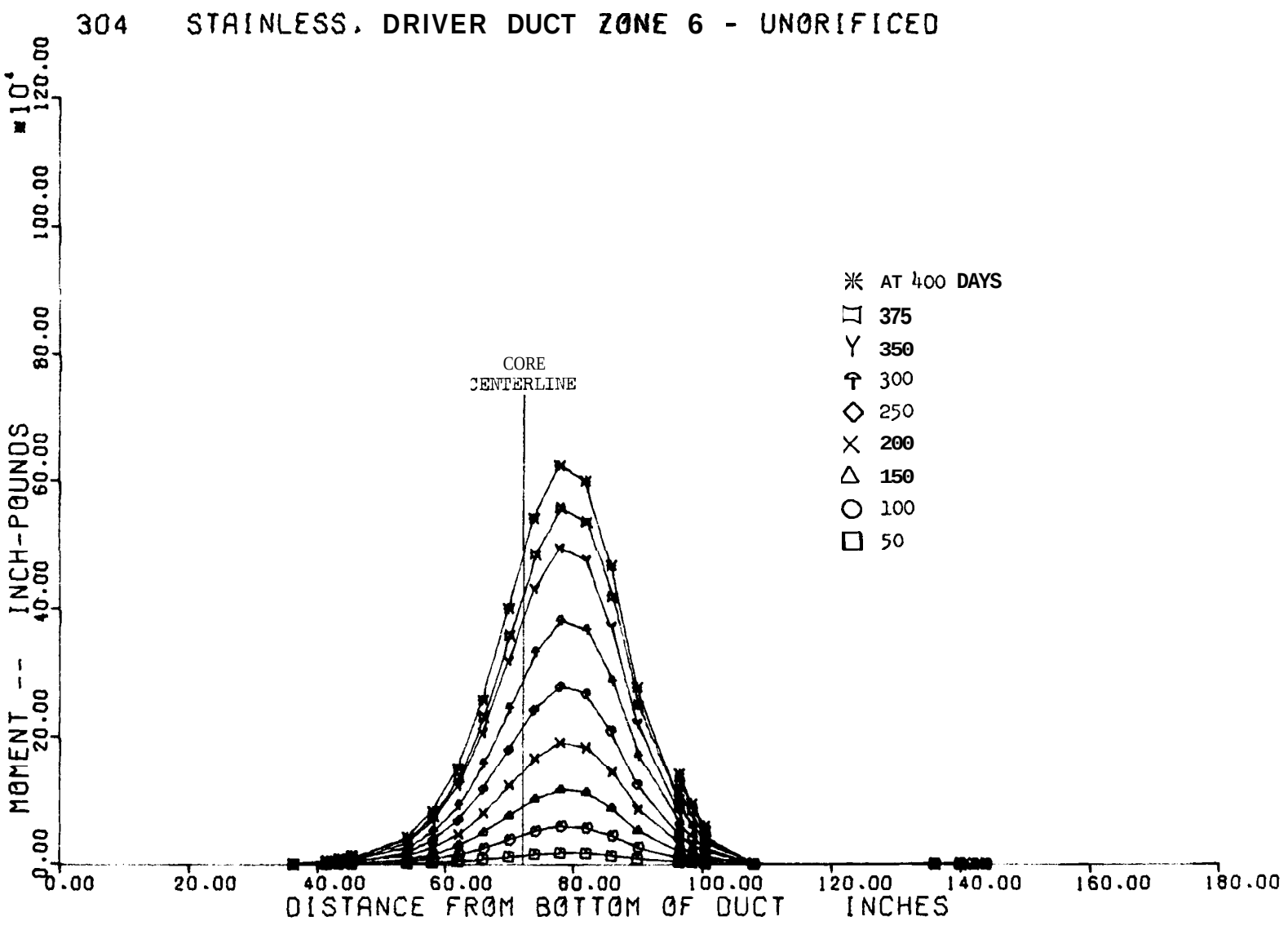

FIGURE 14. Applied **Moments on Row 6** Driver **Duct**

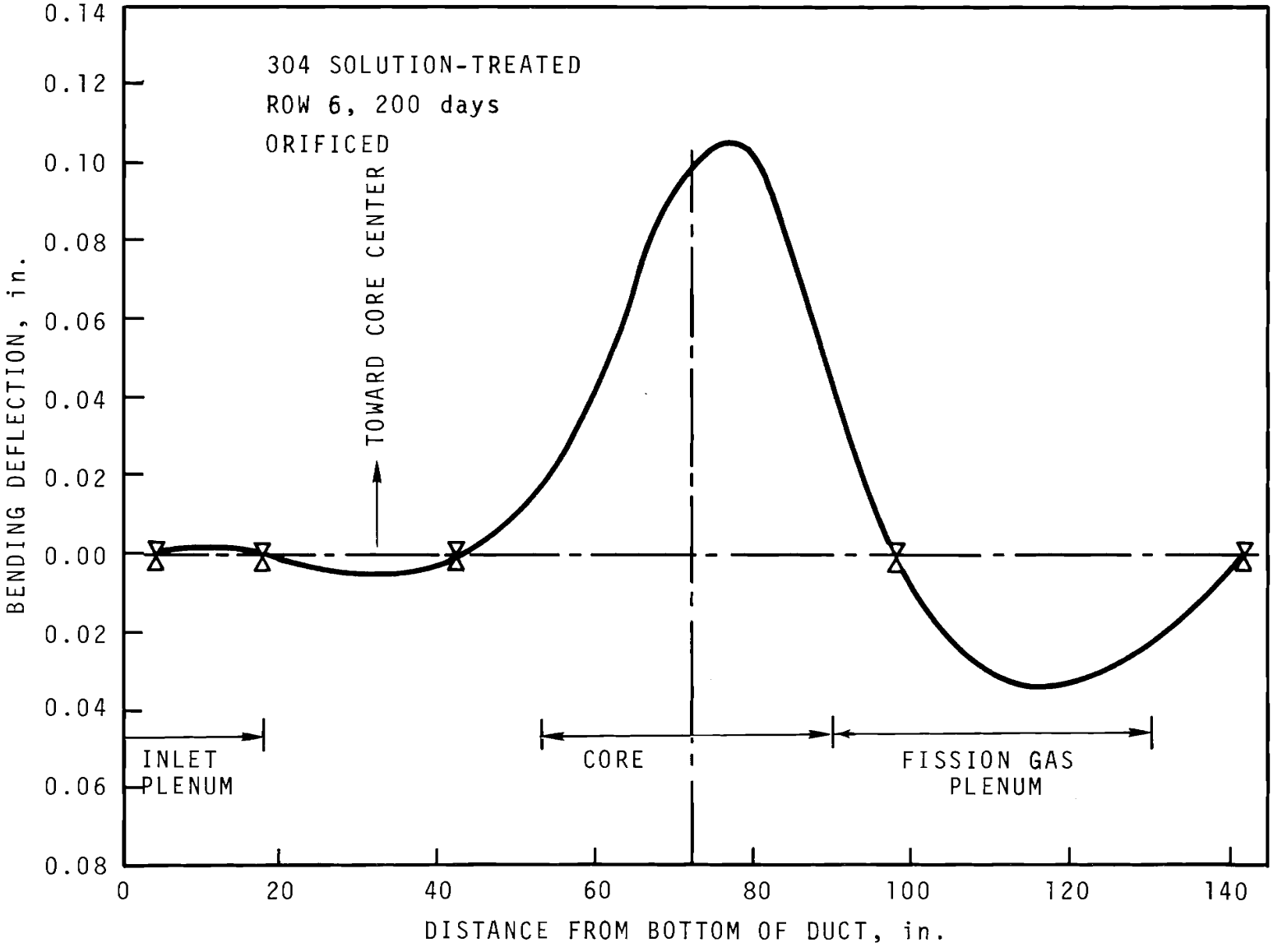

FIGURE 15. Driver Duct Deflection

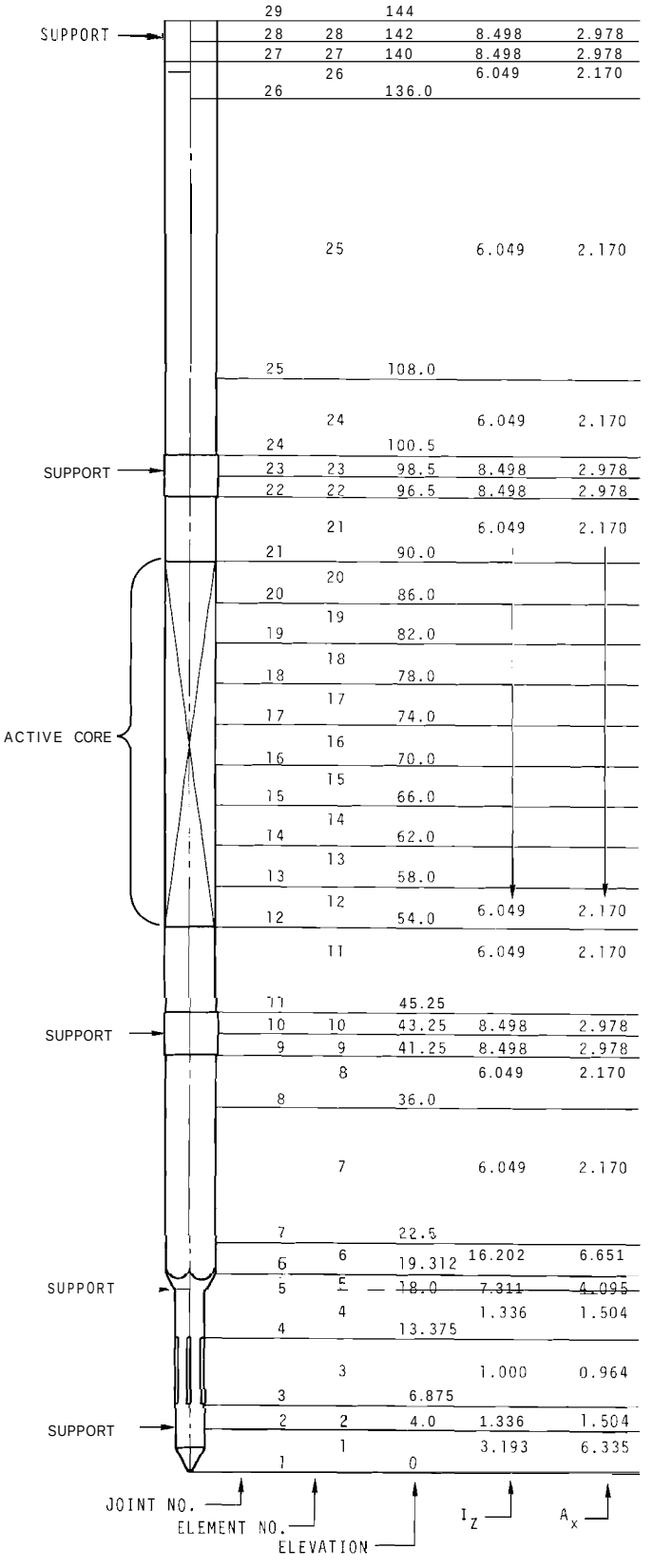

FIGURE 16. Fuel Assembly and Control Assembly Outer Duct

TABLE 2. 304 Driver Duct Deflection Based upon Elastic Analysis

Component Driver Ducts	In-Core Deflection, in. 200 Days	300 Days	400 Days	Duct Top Deflection, in. 200 Days	300 Days	400 Days
Row 1	0.000	0.000	0.000	0.000	0.000	0.000
Row 2	0.035	0.072	0.119	0.887	1.781	2.918
Row 3	0.065	0.130	0.214	1.602	3.212	5.260
Row 4	0.085	0.172	0.254	2.099	4.211	6.263
Row 5	0.094	0.189	0.308	2.311	4.633	7.584
Row 6	0.104	0.206	0.336	2.537	5.071	8.292

TABLE 3. 316 Driver Duct Deflection Based upon Elastic Analysis

Component Driver Ducts	In-Core Deflection, in, 200 Days	300 Days	400 Days	Duct Top Deflection, in. 200 Days	300 Days	400 Days
Row 1	0.000	0.000	0.000	0.000	0.000	0.000
Row 2	0.010	0.021	0.034	0.263	0.523	0.852
Row 3	0.018	0.038	0.062	0.479	0.951	1.548
Row 4	0.024	0.050	0.081	0.617	1.228	2.000
Row 5	0.028	0.056	0.091	0.695	1.381	2.248
Row 6	0.034	0.067	0.109	0.833	1.651	2.685

equivalent to a 50 °F decrease in bulk outlet temperature), the maximum swelling for this lower temperature case, would be only 83% of the value for the reference core. Because the maximum swelling location is below the core top, the corresponding temperature decrease associated with the maximum swelling location is only 33 °F. Similarly, a 100 °F decrease at the core top would result in only 68% of the swelling predicted for the reference core.

CONTROL RODS

The radial dilatations and the duct length increases for the control rods are tabulated in Table 4. The values are all

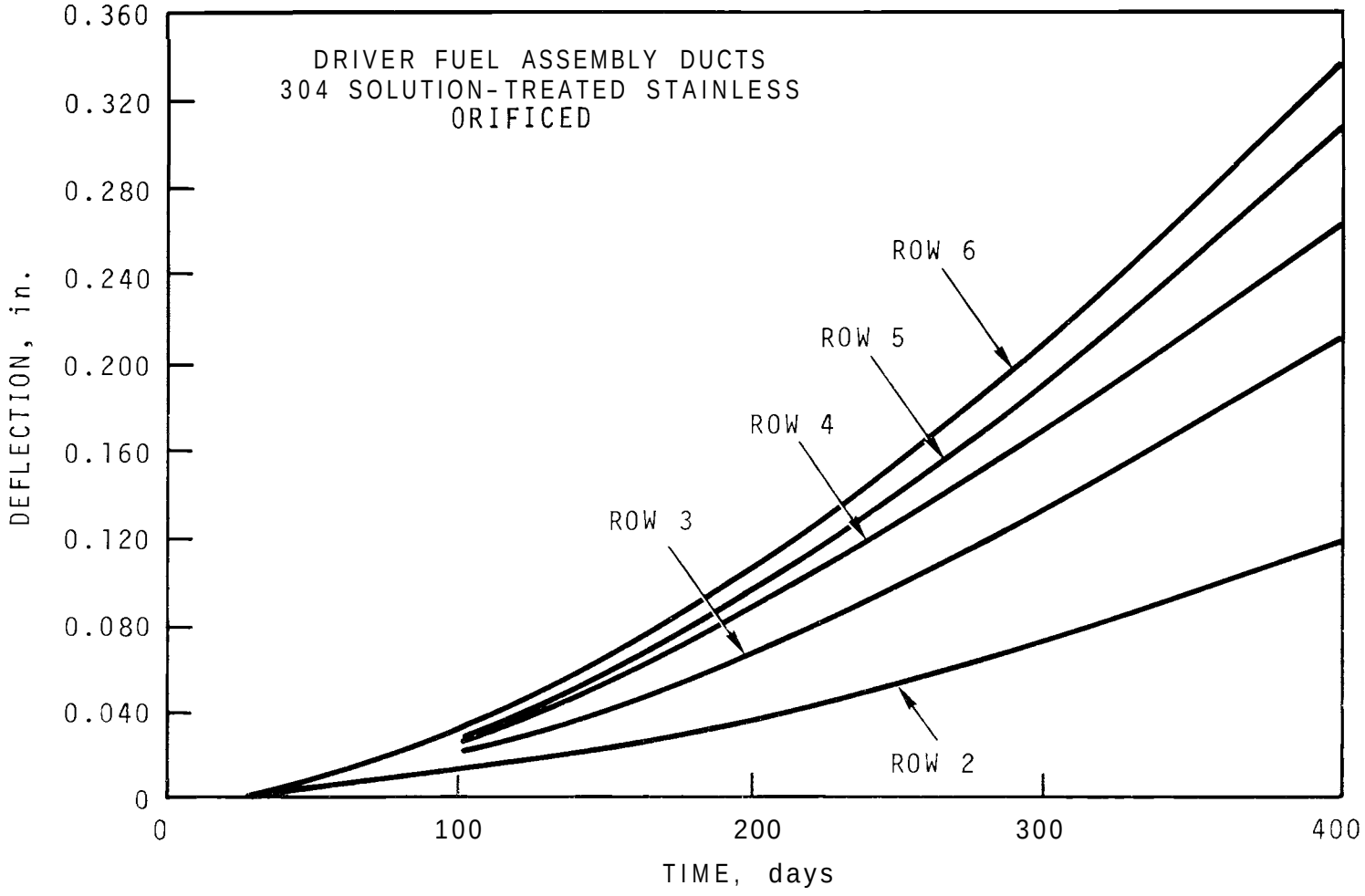

FIGURE 17. In-Core Deflection During Operation

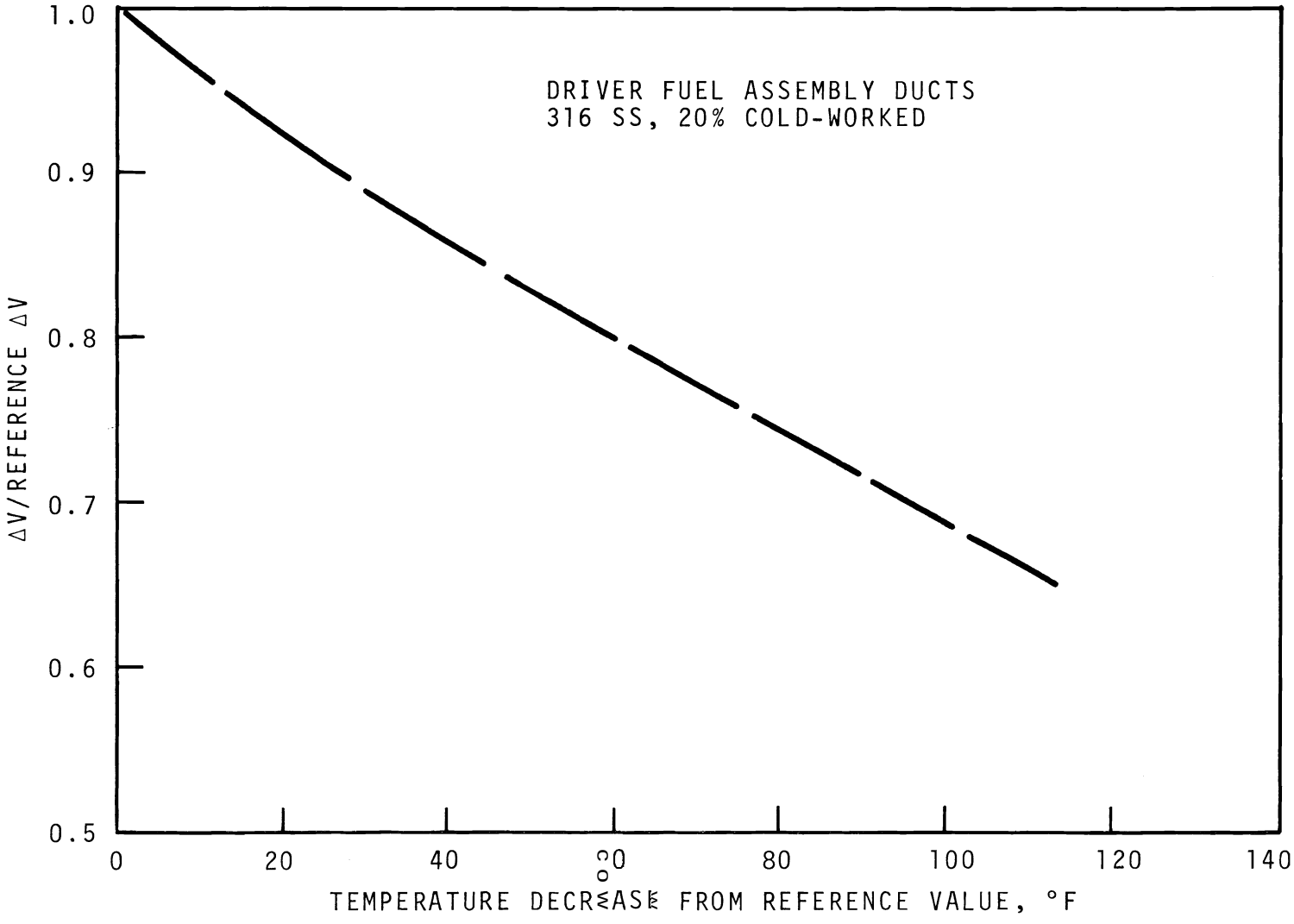

FIGURE 18. Effect of Duct Wall Temperature Swelling

TABLE 4. Predicted Swelling, 316 Cold-Worked Control Rods

Component	Peak Fluence, 10^{22} nvt	Maximum $\Delta V/V$, %	Dilatation (ΔR), in.			Duct Length Increase (ΔL), in.		
Control Rods	400 Days	400 Days.	200 Days	300 Days	400 Days	200 Days	300 Days	400 Days
Row 4:								
Guide Tube	13.3	1.5	0.003	0.006	0.010	0.088	0.108	0.134
Inner Duct	13.3	1.5	0.003	0.006	0.009	0.077	0.094	0.116
Row 5:								
Guide Tube	11.5	1.2	0.002	0.005	0.008	0.065	0.080	0.099
Inner Duct	11.5	1.2	0.002	0.004	0.007	0.057	0.069	0.085
Row 7:								
Guide Tube	5.7	0.4	0.001	0.001	0.002	0.021	0.025	0.032
Inner Duct	5.7	0.3	0.000	0.001	0.001	0.016	0.019	0.024

lower than for the corresponding material and location of a driver fuel assembly duct because of the lower temperature in the control rod ducts.

In all cases, the inner duct is predicted to swell less than the surrounding guide tube. This provides additional clearance to prevent binding of the control rod during operation. The required diametral clearance between the control rod guide tube and the inner duct to prevent binding of these two components is determined by their swelling distortion. The major effect is the bending of the inner duct (Table 5). The required clearance is the sum of the increased envelope of the inner duct and the decreased envelope inside the guide tube. This change in envelope is largely determined by the bending deflection from differential swelling. The guide tube

TABLE 5. Control Rod Deflection Based upon Elastic Analysis

Component	In-Core Deflection, in.			Duct Top Deflection, in.		
Control Rods	200 Days	300 Days	400 Days	200 Days	300 Days	400 Days
Row 4:						
Guide Tube	0.013	0.025	0.043	0.228	0.452	0.735
Inner Duct	0.067	0.133	0.218	-	-	-
Row 5:						
Guide Tube	0.015	0.031	0.050	0.269	0.534	0.869
Inner Duct	0.078	0.156	0.258	-	-	-
Row 7:						
Guide Tube	0.008	0.016	0.027	0.204	0.415	0.685
Inner Duct	0.062	0.124	0.202	-	-	-

deflection of concern is that associated with the duct when supported as indicated in Figure 16. The inner duct is supported only at the top; any additional supports would create a binding situation. The required clearances are shown in

Figure 19. The required clearance depends upon the fixity of the top support. As presently designed, the required diametral clearances are about 1 1/2 and 3/4 in. for 304 solution-treated and 316 cold-worked, respectively, at 400 days exposure. If the life of the control rod is restricted to 2 1/2 months because of fission gas pressure limitations, the corresponding required diametral clearances are about 0.100 and 0.030 in. All of these values can be reduced to about 1/2 their stated value by proper design of the inner duct upper support (Figure 19).

CLOSED LOOPS

The radial-dilatation and axial-length increase for 316 cold-worked closed-loop components is tabulated in Table 6. Values for 304 solution-treated stainless are higher by a factor of about 1.7 for the closed loop temperatures. At these higher closed-loop temperature, about twice the swelling occurs compared with corresponding driver ducts.

The flow tube liner is predicted to expand 0.053 in. radially while the flow tube surrounding it is predicted to swell only 0.030 in. The effect of this crushing type of interaction on the insulation separating these two concentric components must be investigated in detail. The flow tube liner is predicted to increase in length by 1.057 in. while the flow tube is predicted to expand axially only 0.570 in. In principle, this difference in axial expansion has been provided for with metal bellows connecting the bottom of these two components. However, the restraint to axial movements, which results from the crushing interaction of these two components, will reduce the effectiveness of this bellows connection. Therefore, the effectiveness of the bellows feature must be analyzed in detail. The in-core deflection of the closed loops is predicted to be about twice the deflection of corresponding driver ducts.

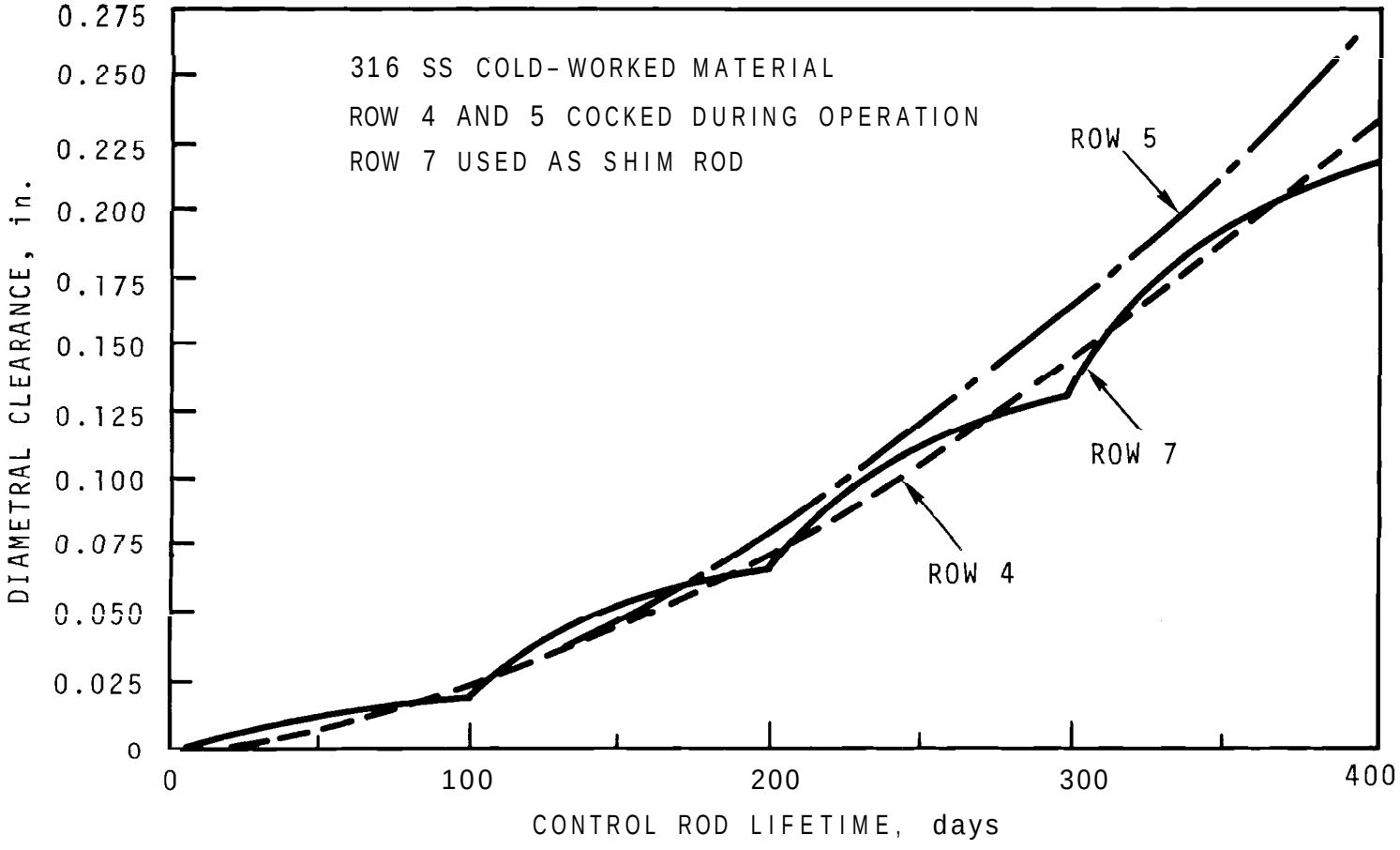

FIGURE 19. Required Control Rod Clearance

TABLE 6. Predicted Swelling in 316 Closed Loop Components (316 20% CW Ducts Orificed)

Component	Peak Fluence, 10^{22} nvt	Maximum ΔV/V, %	Dilatation (ΔR), in.			Duct Length Increase (ΔL), in.		
Closed Loop	400 Days	400 Days	200 Days	300 Days	400 Days	200 Days	300 Days	400 Days
Row 2								
Pressure Tube	15.2	7.4	0.017	0.033	0.054	0.443	0.547	0.679
Liner	15.2	7.3	0.014	0.029	0.047	0.452	0.559	0.693
Flow Tube	15.2	6.0	0.009	0.019	0.030	0.372	0.459	0.570
Liner	15.2	12.1	0.016	0.033	0.053	0.696	0.859	1.064
Test Tube	15.2	12.1	0.015	0.030	0.049	0.692	0.853	1.057
Row 6								
Pressure Tube	9.1	3.1	0.005	0.010	0.016	0.131	0.162	0.200
Liner	8.9	2.9	0.004	0.009	0.014	0.136	0.168	0.208
Flow Tube	8.5	2.3	0.003	0.006	0.009	0.112	0.138	0.171
Liner	8.4	4.4	0.005	0.010	0.016	0.209	0.258	0.320
Test Tube	8.4	4.4	0.004	0.009	0.015	0.207	0.256	0.317

All components within each closed loop assembly have similar deflection curves; thus, they nest together and no interaction from bending is predicted.

REFLECTORS

Because the reflectors operate at a lower temperature and in a lower flux environment, they swell much less than fuel assembly driver ducts. The swelling decreases very rapidly with radial position as indicated below.

Row No.	Relative Swelling and Bending
6	1
7	1/4
8	1/12
9	1/36
10	1/360

INTERACTION OF CORE COMPONENTS DURING OPERATION

The fast-neutron-induced dilatation and distortion can cause the clearances between ducts to disappear. When this happens structural interaction between components occurs at locations between the support pads. These interactions can cause reactivity or thermal changes, component malfunction or rupture of components. It is necessary to predict the reactivity and thermal changes during and after operation. To insure against component malfunction or rupture, it is also necessary to understand the mode of interaction and to be able to analyze it.

INTERACTION BETWEEN DRIVER DUCTS

Rigorous analysis of the interaction between ducts requires simultaneous consideration of all driver, control-rod, closed-loop, open-test, reflector, and shield ducts. Although computer codes are not available to do this, an assumed symmetry of the core permits analysis of the interaction between only 6 driver ducts, one in each row (Figure 20). Much insight into component interaction can be gained by this simpler analysis.

To determine when interaction between driver ducts will occur, it is necessary to determine the clearance between ducts as a function of time. This requires consideration of both the radial dilatation and the bending deflection. The relationship between duct clearance, radial dilatation, and bending deflection is illustrated in a scale representation of the axial distribution of duct clearance (Figure 21). The horizontal scale is greatly expanded, and the vertical scale has been greatly contracted. Interaction between duct Rows 1 and 2 occurs about 6 in. above the core mid-plane. Illustrating the clearances and duct deflection shapes in the core region only, Figures 22, 23, and 24 represent times corresponding to just prior to initial duct interaction, shortly after initial

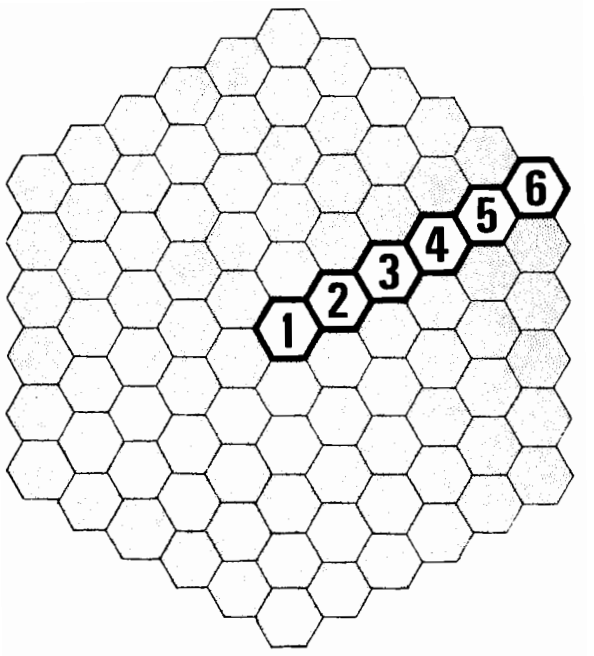

FIGURE 20. Location of Driver Ducts Analyzed

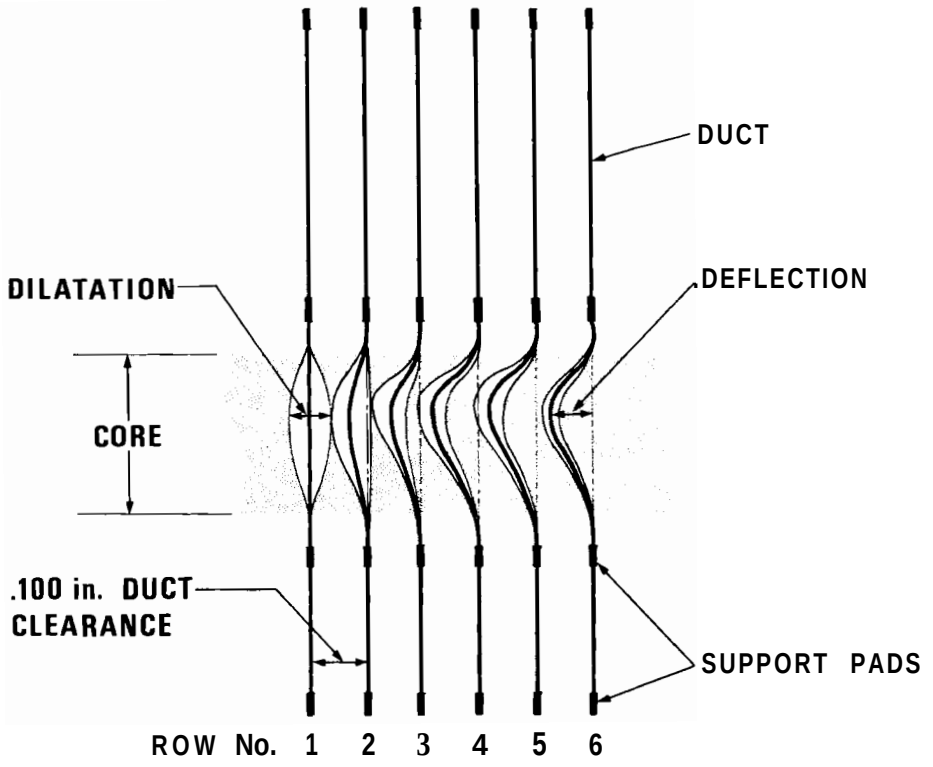

FIGURE 21. Relationship Between Duct Clearance, Dilatation and Deflection

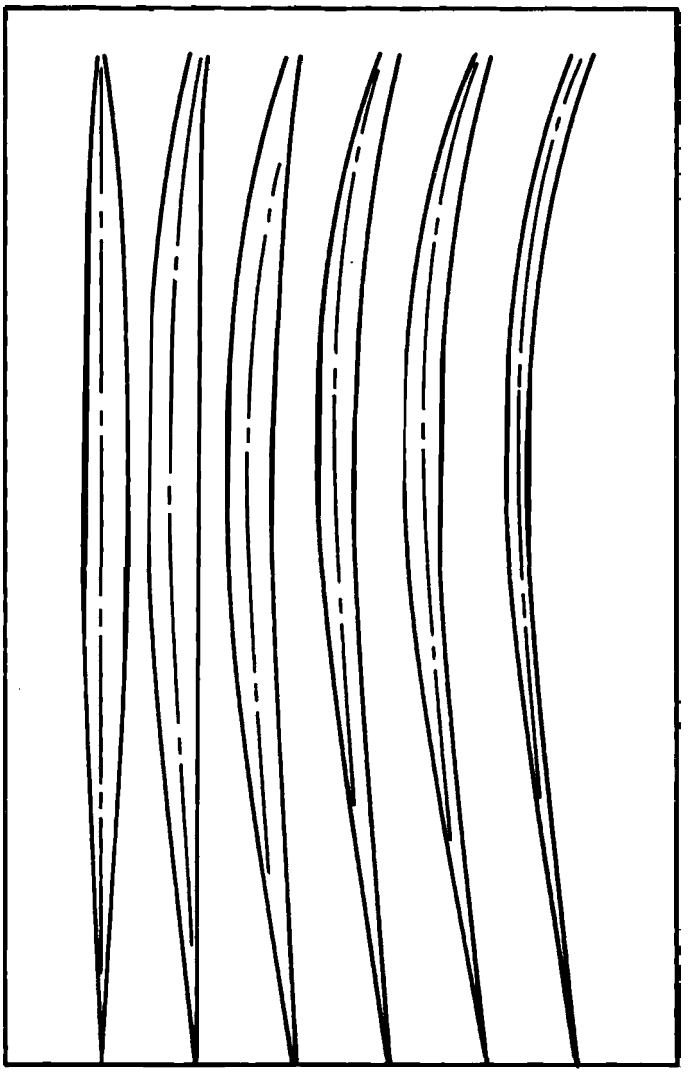

FIGURE 22. Effect of Metal Swelling on Duct Behavior - 200 Days, 304 Solution-Treated Orificed Core

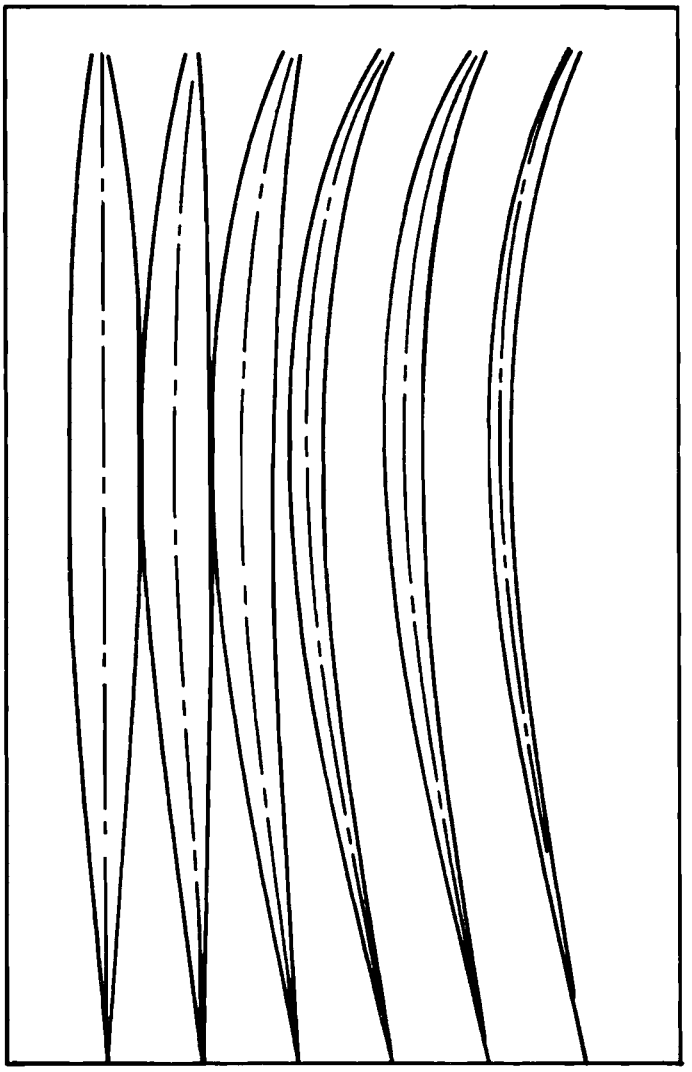

FIGURE 23. Effect of Metal Swelling on Duct Behavior - 225 Days, 304 Solution-Treated Orificed Core

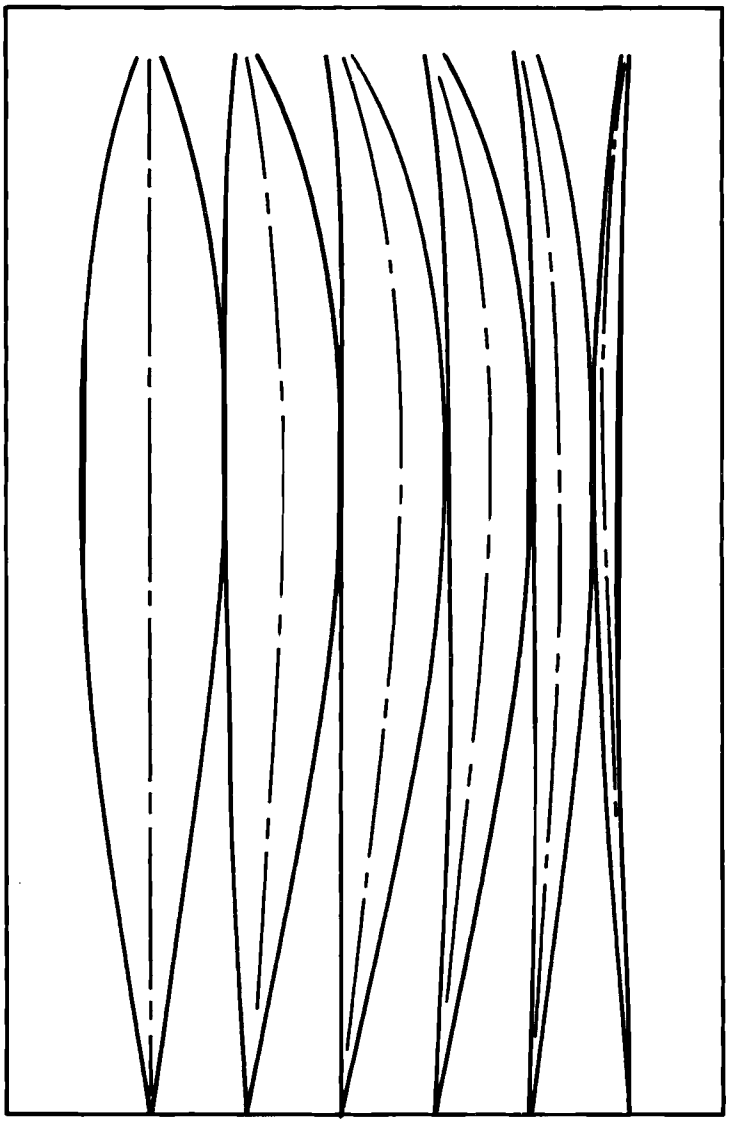

FIGURE 24. Dilatation and Bending 304 Solution-Treated, 325 Days

duct interaction, and after much duct interaction, respectively. This elastic analysis predicts that all ducts, except Row 1, bow inward prior to interaction. Because of symmetry, Row 1 remains straight even after duct-to-duct interaction. Therefore, except in Row 1, any additional dilatation after duct-to-duct contact causes a reverse or outward bending movement of all contacting ducts. As illustrated, this reverse bending is predicted to start occurring at about 220 days in Row 2. After this exposure, the material will have a fluence of approximately 1×10^{23} nvt total, a very limited ductility and, thus, a very limited ability to accommodate this reverse bending without rupture of the duct walls. Therefore, duct-to-duct contact appears to be tantamount to duct failure. It can be noted that dilatation is the major problem in the central ducts. In contrast, bending deflection is the major problem in the peripheral ducts. This indicates duct rotation will be helpful in Rows 5 and 6 to straighten these ducts during operation but will be ineffective in the center rows.

Figure 25 shows the predicted clearance between ducts as a function of time, with the clearance between Rows 1 and 2 going to zero in 220 days (indicating a burnup limitation) and Rows 2 and 3 to zero in 240 days. However, if the swollen Row 1 duct were still in the core, it would cause an outward movement of the Row 2 duct after 220 days. Such a movement would cause the clearance between Rows 2 and 3 to close faster, and the clearance would go to zero in 228 days (as indicated by the dashed lines). Figure 25 indicates that Rows 1, 2 and 3 would have to be replaced after 200 days to prevent failure before 300 days. Rows 4 and 5 would need to be replaced in 300 days because they are predicted to interact in 380 days at which time they have burnups of about 50,000 to 60,000 MWd/tonneM. Obviously, duct rotation would change these relationships to increase the burnup limitation in the outer rows.

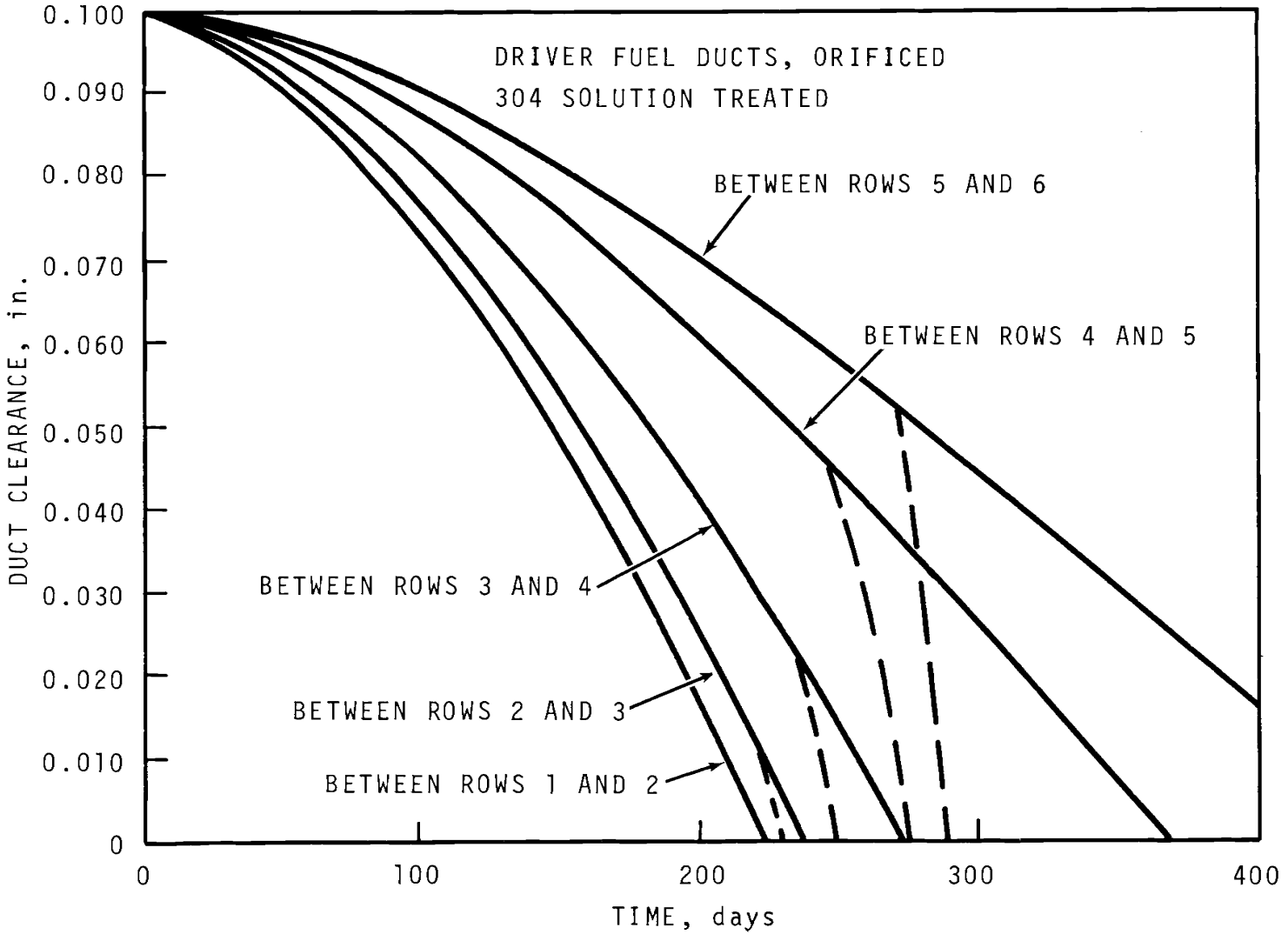

FIGURE 25. Clearance Between 304 Ducts

No duct-to-duct interactions are predicted for 316 cold-worked driver fuel assembly ducts shown in Figure 26.

INTERACTION BETWEEN DRIVER DUCTS AND CONTROL RODS

Figure 27 illustrates the predicted clearances if cold-worked 316 control-rod guide tubes are substituted for cold-worked 316 driver-fuel assembly ducts in Rows 4 and 5. The predicted clearances resulting from control rods in these rows is larger than if driver ducts were in these rows.

INTERACTION BETWEEN DRIVER DUCTS AND CLOSED LOOPS

Figure 28 indicates that interactions occur if cold-worked 316 closed loops are substituted for the cold-worked 316 drivers in Rows 2 and 6. The Row 2 closed loop causes a closed-loop driver duct interaction in about 320 days. Independently, the Row 6 closed loop causes a similar interaction in 280 days (about 40,000 MWd/tonneM). Thus, even though these closed loops are not in the same radial row (as is assumed in this analysis), the predictions of interaction are still valid because the interactions are independent. These duct-to-duct interactions are a result of the large swelling induced bending in the closed loops.

INTERACTION BETWEEN DRIVER DUCTS AND INSTRUMENT TREE

The 304 solution-treated driver-fuel assembly ducts are predicted to increase in length approximately 0.8 in. at goal burnup. The 316, 20% cold-worked ducts are predicted to increase 0.334 in. Although the instrument tree is not presently designed to accommodate these length increases, the appropriate modifications to the design will probably be simple to accomplish.

INTERACTION BETWEEN DRIVER DUCT AND REFLECTORS

Relatively straight ducts in Rows 7, 8 and 9 result from a minimal swelling and bending in the reflector ducts. Contact is not predicted in these components until after 1,000 days. Duct-to-duct contact between a driver duct in Row 6 and a reflector

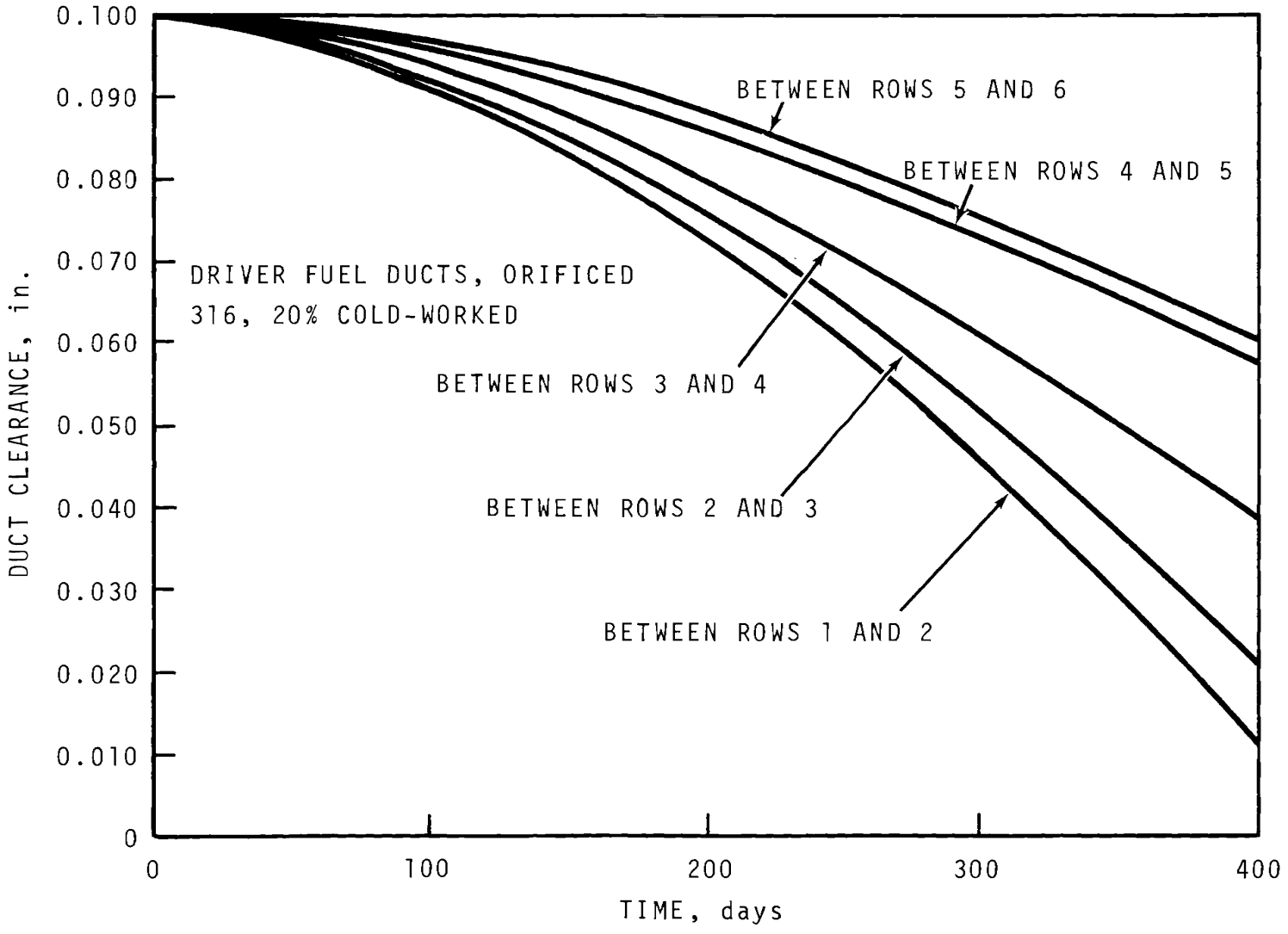

FIGURE 26. Clearance Between 316 Ducts

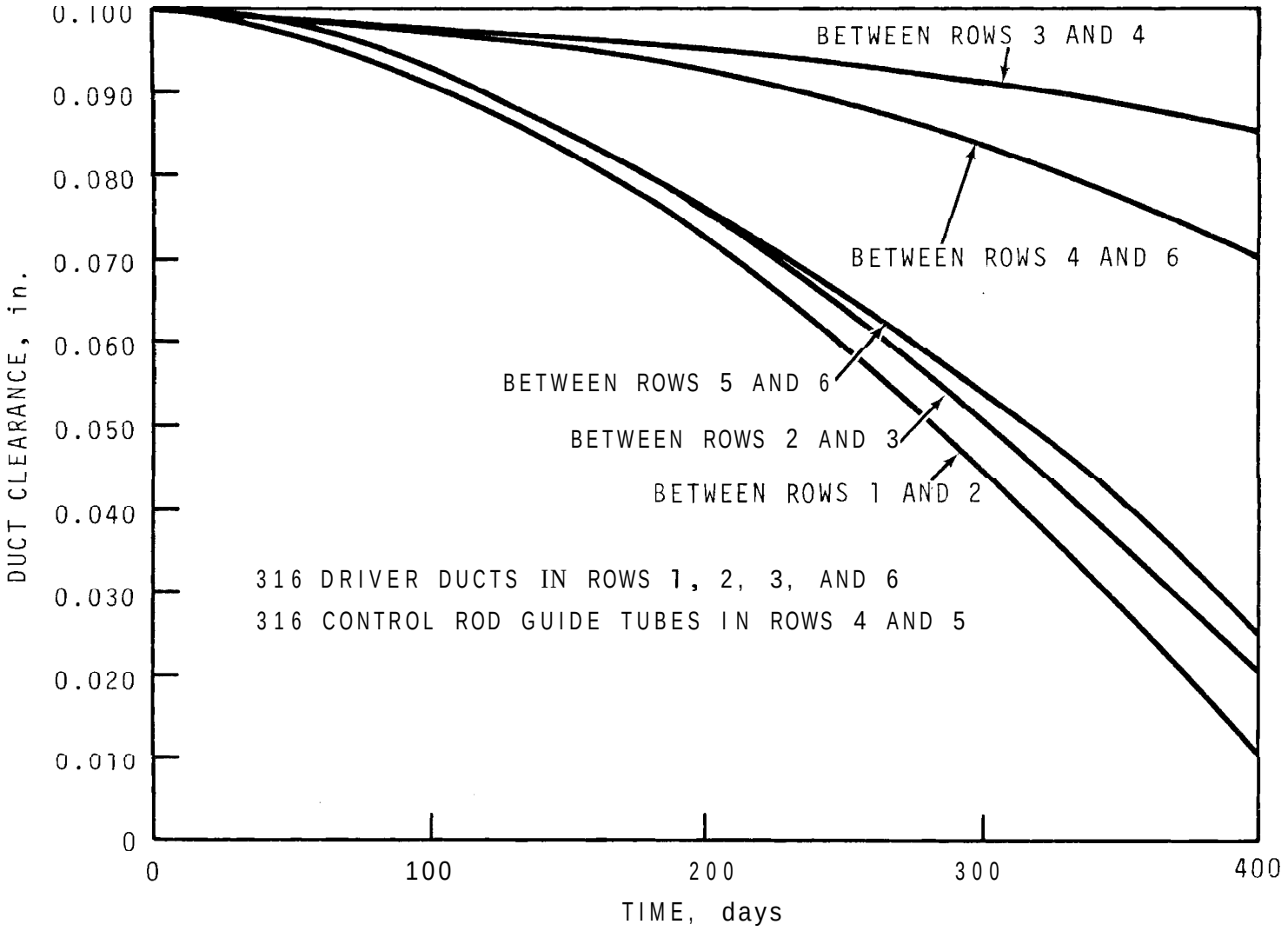

FIGURE 27. Clearance Between Driver **Ducts** and Control Rods

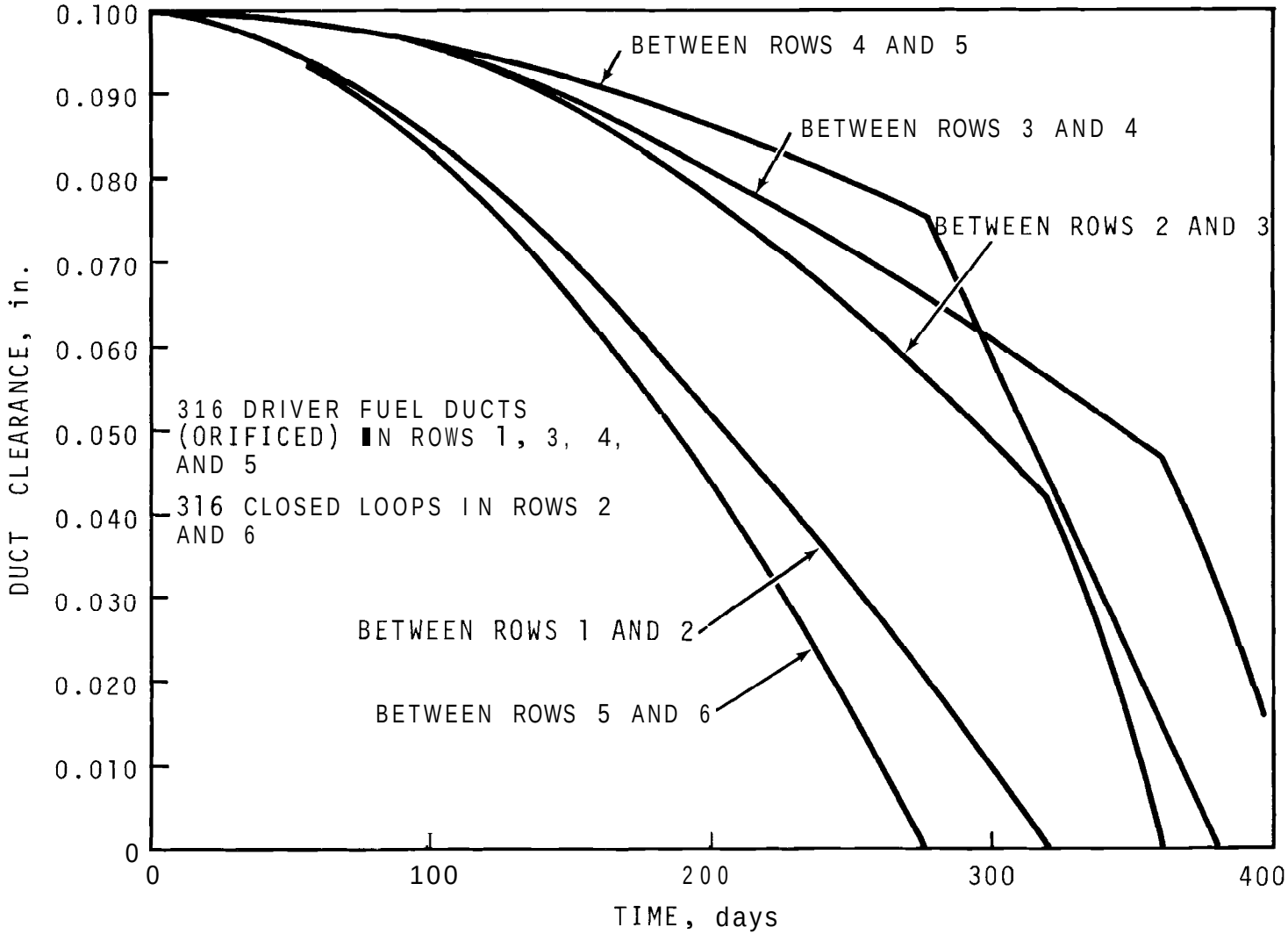

FIGURE 28. Clearance Between Driver Ducts and Closed Loops

in Row 7 depends upon the fuel management scheme in Row 6; thus, no meaningful prediction is presently practical.

EFFECT OF CREEP ON COMPONENT INTERACTION

Analysis of the creep effect on in-core duct deflection requires a computer code presently under development. Creep is expected to have a minor effect upon the slow in-core deflection values resulting from differential swelling.

REACTIVITY CHANGE DUE TO CORE DISTORTION

During operation, the fuel expands axially. Simultaneously, the fuel is moved radially inward toward the core center (prior to duct contact, at least) by duct deflection from differential swelling. These two effects tend to offset each other with respect to reactivity change; however, a net reactivity increase of about 0.5% is predicted.

EFFECTS OF CORE LENGTH

One method of reducing the magnitude of in-core deflections is to reduce the core length. Figure 29 indicates that a 30 in. core would have only 0.78% as much deflection as a Reference 36 in. core. An indication that the deflection ratio decreases faster than the core length ratio is based upon a first assumption that the core is centered between its immediately adjacent supports (Figure 29). The required location of these supports depends upon the axial flux and temperature distribution. Although the supports are located as far removed from the core as practical to reduce swelling of the support pads, they still must be located reasonably close to provide a negative temperature coefficient. Further analysis might indicate that the lower core support could be moved closer to the core which would reduce the predicted in-core deflections.

Any reduction of core length would decrease the magnitude of the interaction between all core components.

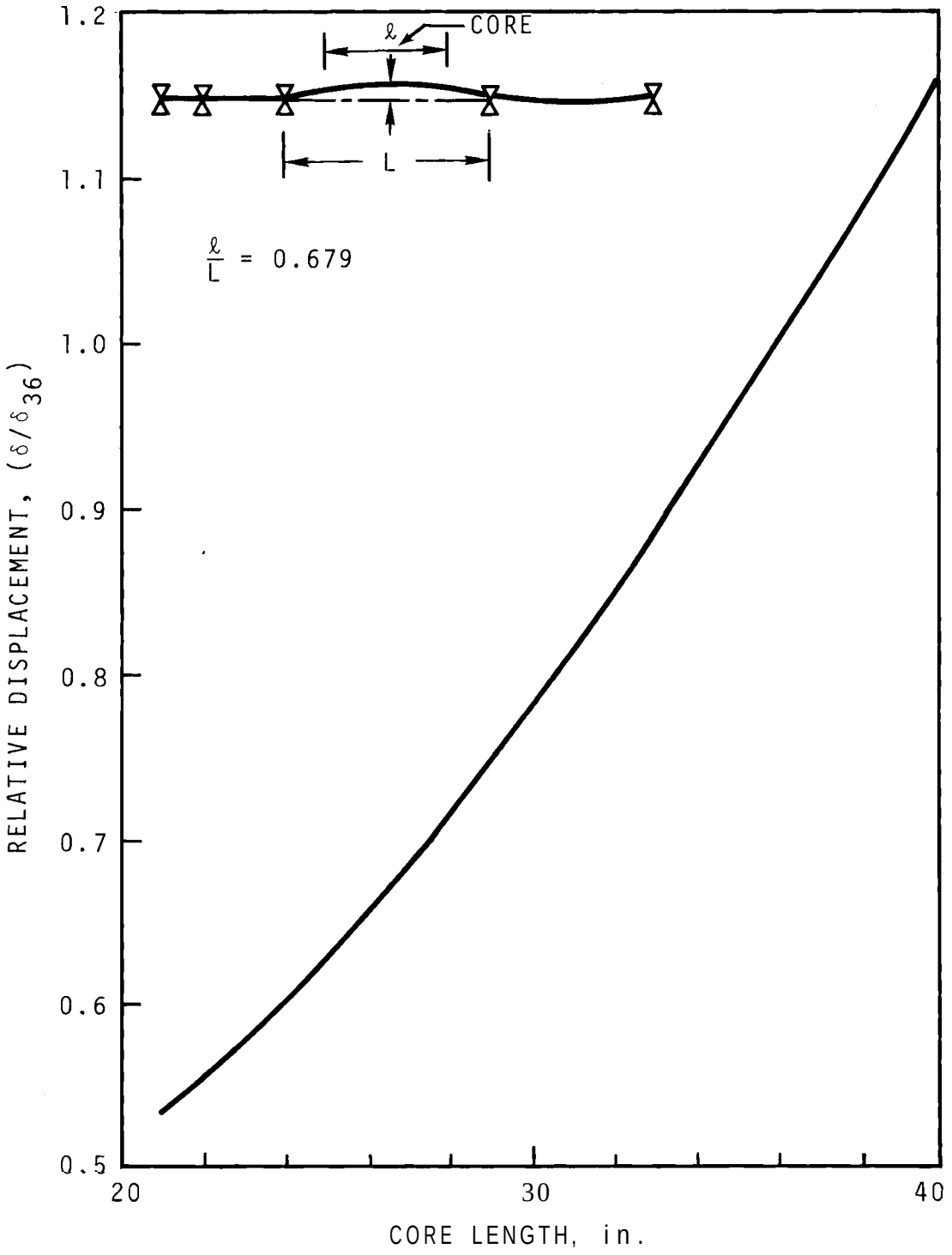

FIGURE 29. Effect of Core Length on Core Deflection

EFFECT OF DUCT ROTATION

Rotating the ducts 180° at intervals during their life greatly reduces the predicted elastic bending deflection, as illustrated in Figure 30 which compares the predicted displacement for a rotated and nonrotated cold-worked, 316 stainless, Row 6 driver duct. This figure presents the duct movement in terms of displacement instead of clearance because some assumption regarding fuel management is necessary before clearances can be calculated. If the adjacent duct wall is assumed as a fixed straight wall, the clearance can be considered as 0.100-displacement.

The duct wall displacement results from the combined effect of duct deflection (δ) and radial dilatation (ΔR) as previously discussed in this section (Interaction Between Driver Ducts). The magnitude of these individual contributions to duct wall deflection is shown as dashed lines in Figure 30. The solid lines represent the combined effect of bending and radial dilatation. It may be noted that the rotated duct is predicted by elastic analysis to have about 0.040 in. maximum displacement over the 600 day period compared with about 0.250 in. displacement for the nonrotated duct. Also, after 600 days, radial dilatation becomes significant in Row 6. This particular case is not optimum because very little reduction in deflection is gained by the rotation at 200 and 400 days. Obviously, additional study to determine the trade off between reactor down time and extending the burnup life of core components is required.

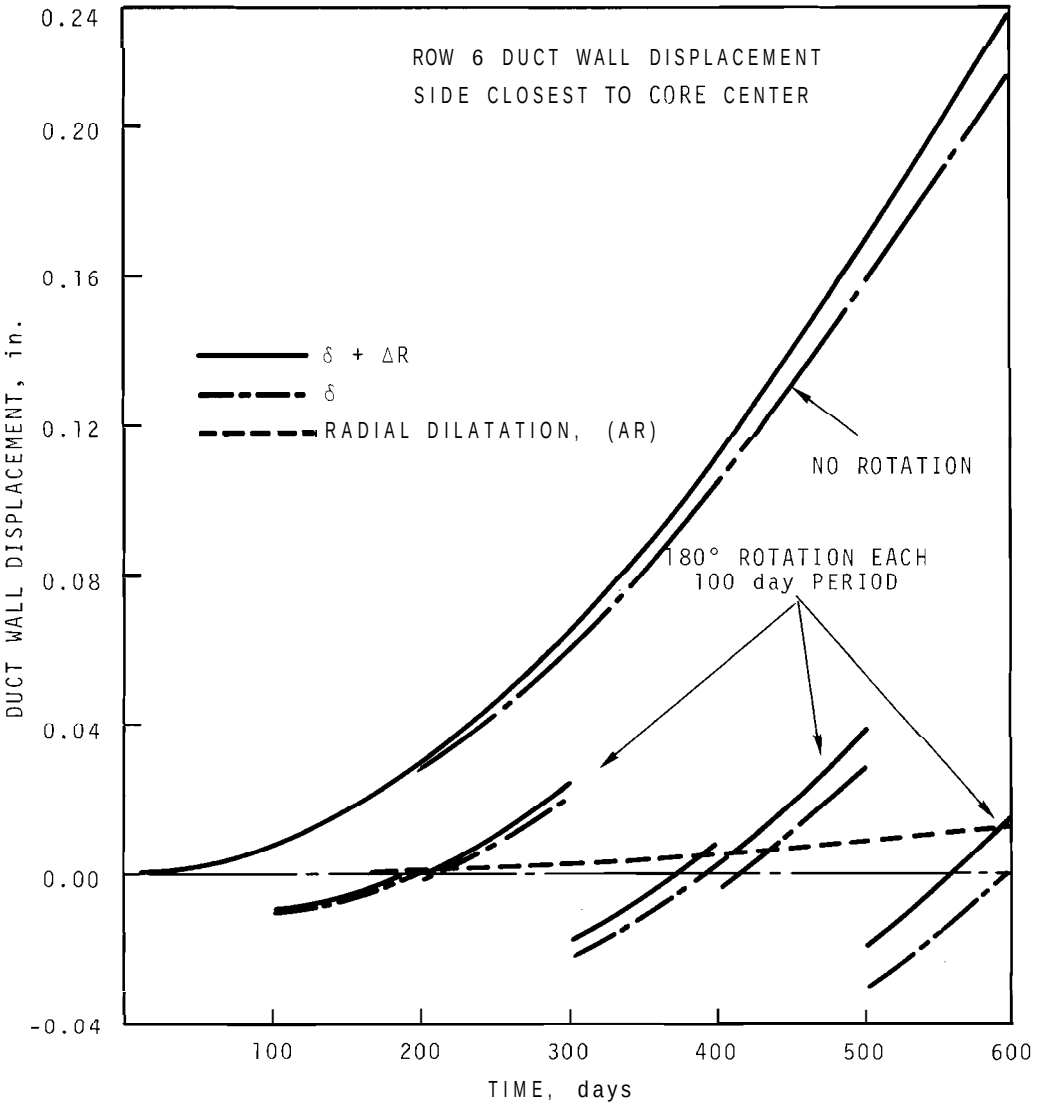

FIGURE 30. Effect of Duct Rotation on Displacement

COMPONENT INTERACTION DURING REFUELING

Prior to insertion or withdrawal of the in-core assemblies from the core, the core clamping system must be released to provide sufficient clearance. With the restraint mechanism released, the in-core component distortions result in an outward displacement of duct tops. If the total core were made up of driver assemblies, with no creep occurring, the result would be a "petalled" deformation pattern similar to that shown in Figures 31 and 32. The introduction of control rods, safety rods, and closed loops, results in a nonsymmetric pattern because 1) the control and safety rods have less deflection than the drivers and 2) the closed loops have more deflection and are stiffer than the drivers.

The prime uncertainty with the released array concerns the ability to insert and withdraw a duct without damaging the adjacent elements remaining in the core. Present fuel handling requirements specify that the In-Vessel Fuel Handling Machine (IVHM) must be able to locate a fuel element within a 1/2 in. radius of the predetermined end of life position. By use of calibrated swelling and creep formulations, the theoretical position can be established within this 1 in. diameter range. Therefore duct top locations for IVHM attachment do not appear to be the controlling criterion; instead it may be the ability to insert and withdraw, the IVHM grapple. For purposes of this study, however, the ability to insert the instrument probe of the instrument tree has been selected as the controlling criterion.

The present reference duct has a diametral opening of 4.185 for inserting the instrument probe. The radius of 0.06 on the nose of the pilot blades of the instrument probe allows a maximum duct top displacement of about 2 1/8 in. and this value (for purposes of this study) has been selected as the limiting case for allowable duct top deflection during refueling.

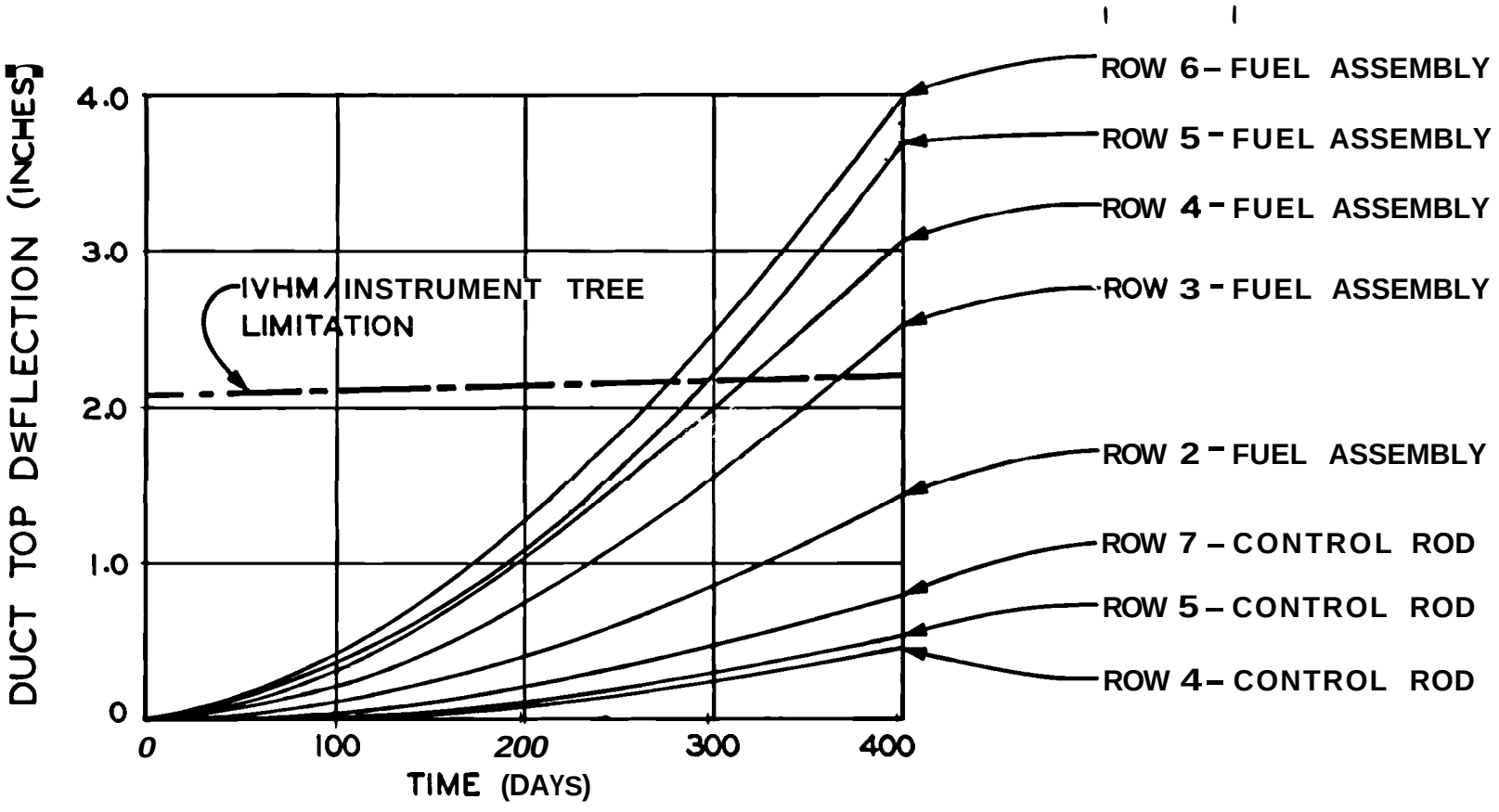

FIGURE 31. Predicted 304 Duct Top Deflection Based upon No Component Interaction

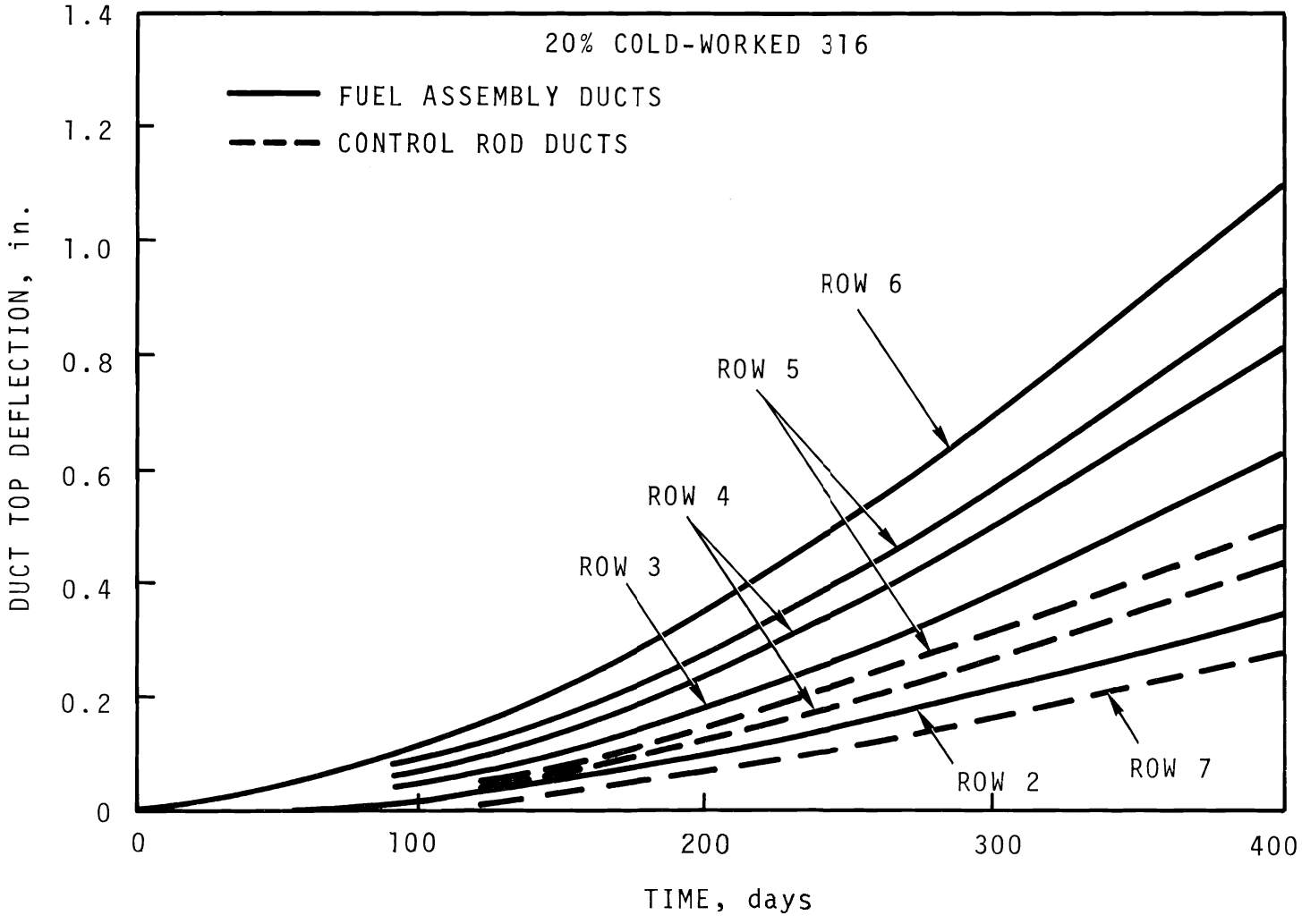

FIGURE 32. Predicted Duct Top Deflection Based upon No Component Interaction

Other potential limiting deflections include limitations imposed by the ability to reinsert reliably the new, straight assembly into the hole pattern. (The duct, restraining its neighbors prior to removal, springs back.)

Another major concern involves the bridging of assemblies during reassembly of the core just prior to startup. With the nonuniform pattern of ducts and the potential for bridging at one in every seven positions, the potential for noncompaction may be high.

DUCT TOP DEFLECTION ANALYSIS

Duct top deflections based upon no interaction with adjacent ducts are shown in Figures 31 and 32 as a function of exposure time for 304 solution-treated ducts and for 316, 20% cold-worked material; fuel handling and instrument probe problems are negligible based on the criterion chosen above. For 304 solution-treated ducts, the 2 1/8 limitation is imposed upon Kow 6 drivers at about 280 days exposure; Rows 5, 4 and 3 driver ducts at 300, 320, and 380 days, respectively. By rotation of ducts in these rows, these deflections could be reduced. It should be noted the total deflection shown is based upon no interaction between components. The actual duct top displacements of the driver ducts is limited by the relatively stiff closed loops and by the control and safety rods whose deflection is significantly less than the driver ducts. In addition, the three reflector rows tend to create a "fence" around the active core because of their reduced deflections. The resultant deflection of all ducts in this partially restrained array was approximated by using an iterative graphical technique. Two patterns of assemblies were considered: SK 3-14715 assumes that the shield row was spaced 0.8 in. from the outer reflector row, and SK 3-14716 assumes that the outer reflector row was able to achieve an unrestrained equilibrium condition with the remaining in-core assemblies. The general assumptions applicable to both cases were:

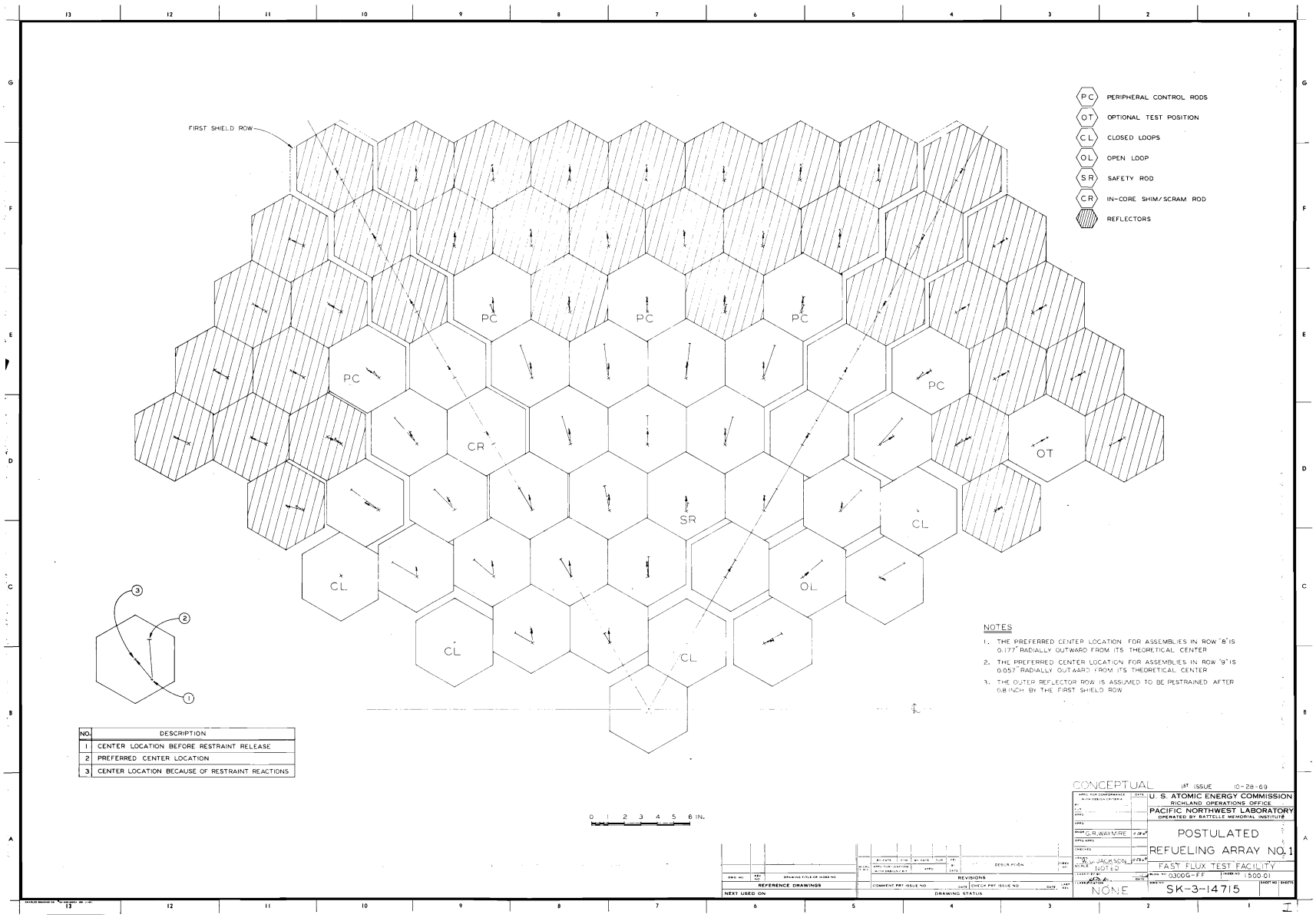
PC PERIPHERAL CONTROL RODS
OT OPTIONAL TEST POSITION
CL CLOSED LOOPS
OL OPEN LOOP
SR SAFETY ROD
CR IN-CORE SHIM/SCRAM ROD
REFLECTORS
FIRST SHIELD ROW
PC
CR
SR
CL
OL
OT
NOTES
1. THE PREFERRED CENTER LOCATION FOR ASSEMBLIES IN ROW "8" IS 0.177" RADIALLY OUTWARD FROM ITS THEORETICAL CENTER
2. THE PREFERRED CENTER LOCATION FOR ASSEMBLIES IN ROW "9" IS 0.057" RADIALLY OUTWARD FROM ITS THEORETICAL CENTER
3. THE OUTER REFLECTOR ROW IS ASSUMED TO BE RESTRAINED AFTER 0.8 INCH BY THE FIRST SHIELD ROW
NO. DESCRIPTION
1 CENTER LOCATION BEFORE RESTRAINT RELEASE
2 PREFERRED CENTER LOCATION
3 CENTER LOCATION BECAUSE OF RESTRAINT REACTIONS
0 1 2 3 4 5 6 IN.
CONCEPTUAL 1ST ISSUE 10-28-69
U. S. ATOMIC ENERGY COMMISSION
RICHLAND OPERATIONS OFFICE
PACIFIC NORTHWEST LABORATORY
OPERATED BY BATTELLE MEMORIAL INSTITUTE
G.R.WAYMIRE
C.W.JACKSON
NOTED
POSTULATED
REFUELING ARRAY NO.1
FAST FLUX TEST FACILITY
WDG. NO. 0300G-FF
IDENT. NO. 1500-01
SK-3-14715
REVISIONS
DESCRIPTION
REFERENCE DRAWINGS
DRAWING STATUS
NONE
NEXT USED ON

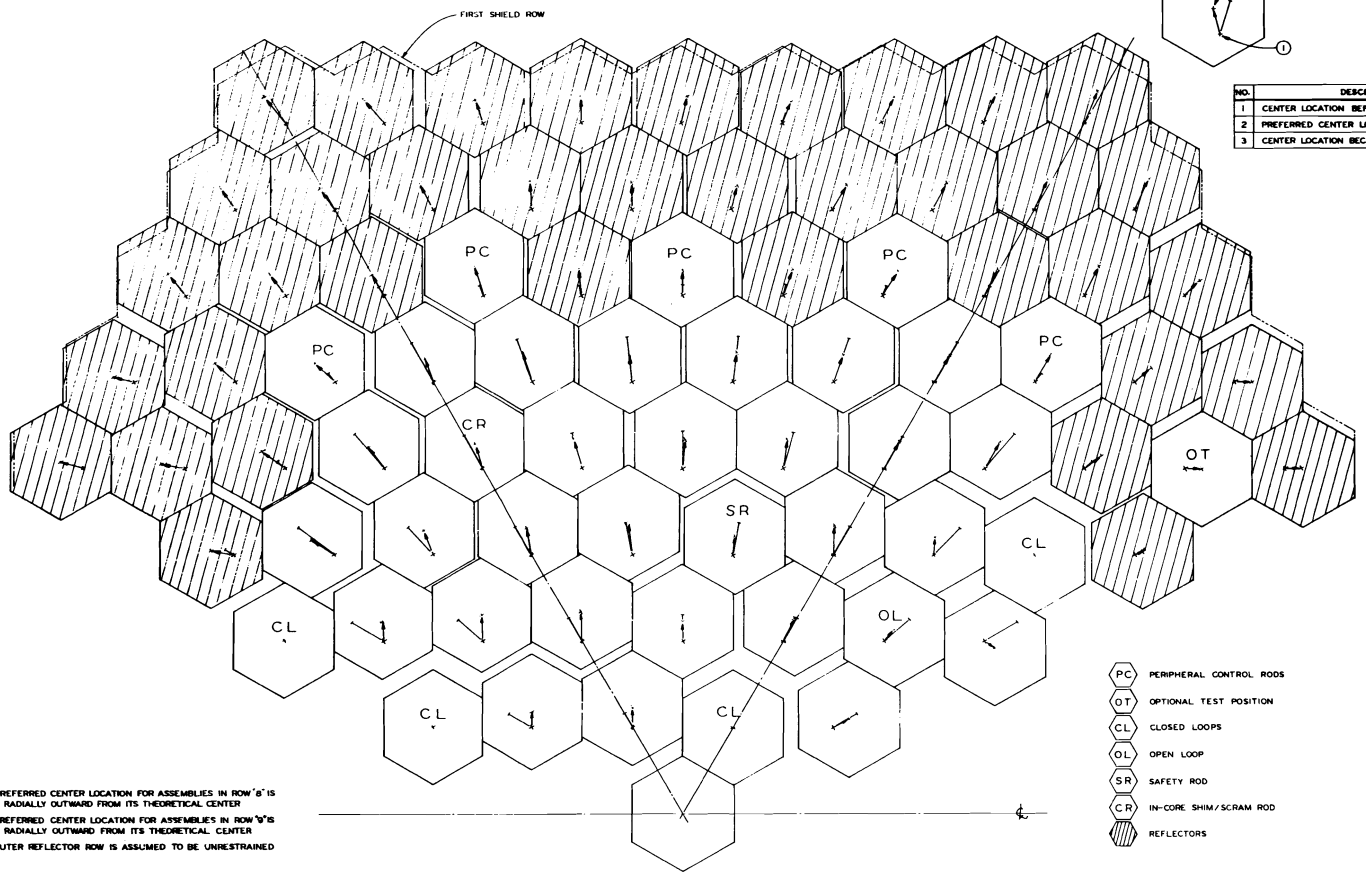

NO.	DESCRIPTION
1	CENTER LOCATION BEFORE RESTRAINT RELEASE
2	PREFERRED CENTER LOCATION
3	CENTER LOCATION BECAUSE OF RESTRAINT REACTIONS

PC PERIPHERAL CONTROL RODS
OT OPTIONAL TEST POSITION
CL CLOSED LOOPS
OL OPEN LOOP
SR SAFETY ROD
CR IN-CORE SHIM/SCRAM ROD
REFLECTORS

NOTES

1. THE PREFERRED CENTER LOCATION FOR ASSEMBLIES IN ROW "8" IS 0.177 RADIALLY OUTWARD FROM ITS THEORETICAL CENTER
2. THE PREFERRED CENTER LOCATION FOR ASSEMBLIES IN ROW "9" IS 0.057 RADIALLY OUTWARD FROM ITS THEORETICAL CENTER
3. THE OUTER REFLECTOR ROW IS ASSUMED TO BE UNRESTRAINED

CONCEPTUAL 1ST ISSUE 10-27-69

U. S. ATOMIC ENERGY COMMISSION
RICHLAND OPERATIONS OFFICE
PACIFIC NORTHWEST LABORATORY
OPERATED BY BATTELLE MEMORIAL INSTITUTE

G.R. WAYMIRE
W.U. JACKSON
NOTED

POSTULATED
REFUELING ARRAY NO. 2
FAST FLUX TEST FACILITY

0.300G-FF 1500.01
NONE SK-3-14716

REFERENCE DRAWINGS
NEXT USED ON
REVISIONS
COMMENT PRT ISSUE NO.
CHECK PRT ISSUE NO.
DRAWING STATUS

BNWL-1286

- Closed loop stiffness was infinite in comparison to the remaining assemblies
- All remaining assemblies have the same stiffness.
- Deflections, shown in Figures 31 and 32, are always radially directed away from the core centerline.

These sketches represent a 1/3 sector array of the duct tops. It may be noted that the duct tops are limited in their radially outward motion when the radial restraint mechanism is released, initially by the reflectors and ultimately by the shield. Certain driver ducts in the core interior are restrained by closed loops and control rods. The closed loops are much stiffer than the driver ducts and are still supported at their top during refueling. Therefore, the driver duct top location during refueling is largely determined by the closed loop location for those ducts near the closed loop. That this closed loop driver duct interaction is independent of the restraint at the core edge may be observed by comparing the postulated driver duct locations around the closed loops in SK 3-14715 and SK 3-14716.

BURNUP LIMITATION CRITERIA

The limitation on fuel lifetime may possibly be determined by the structural performance of core components instead of fuel behavior. Therefore, it is necessary to evaluate potential burnup limiting criteria.

REACTIVITY CHANGE

The net reactivity change appears to be positive. If this reactivity increase is predictable, it will not be a burnup limitation.

REFUELING

The limitation of fuel burnup life associated with refueling may be related to a maximum permitted distortion which is presently undefined.

DUCT CONTACT

Duct-to-duct contact is considered as a burnup limitation. Immediately after duct-to-duct contact, a reverse bending begins--occurring in a duct having a fluence in the 10^{22} range. Since its ductility is immeasurably small, duct-to-duct contact between support pads is undoubtedly a burnup limitation.

CONCLUSIONS

The major conclusions from the study are listed below:

- Burnup limiting duct-to-duct contact is predicted by this elastic analysis to occur before goal burnup in either a 304 solution-treated core or a 316 cold-worked core. The dilatation effects are the primary cause of duct-to-duct contact in Rows 1, 2, and 3. Duct rotation or fuel shuffling will not extend the burnup limit appreciably in these rows. The duct bending effect, primary cause of duct-to-duct contact in Rows 5 and 6, could be reduced by duct rotation.
- Duct top displacement during refueling is very uncertain. Driver ducts are predicted to move radially outward, but are prevented from reaching their stress free location by control-rod guide tubes, closed loops and reflectors. The relatively stiff closed loops play a dominant role in determining the driver duct top locations.

a Because of the large clearances required between the control-rod guide tube and its inner duct, a balanced design is essential for either 304 or 316 SS. This balanced design would reach end of life in the fission gas plenum simultaneously with the end of interduct clearance.

a Row 6, cold-worked 316 closed loops are predicted to swell such that they make contact with adjacent driver ducts in Row 5 at 280 days--a peak burnup of about 40,000 MWd/tonneM. Rotation of the closed loop would increase this life limitation. The testing potential for a Row 6 closed loop needs analysis.

- Because the prediction of swelling is very sensitive to temperature. A metal temperature decrease of 50 °F lowers the predicted swelling by 17% in the driver ducts.

DISTRIBUTION

No. of Copies

OFFSITE

1 AEC Chicago Patent Group

G. H. Lee

31 AEC Division of Reactor Development and Technology

M. Shaw, Director, RDT
Asst Dir for Nuclear Safety
Analysis & Evaluation Br, RDT:NS
Environmental & Sanitary Engrg Br, RDT:NS
Research & Development Br, RDT:NS
Asst Dir for Plant Engrg, RDT
Facilities Br, RDT:PE
Components Br, RDT:PE
Instrumentation & Control Br, RDT:PE
Liquid Metal Systems Br, RDT:PE
Asst Dir for Program Analysis, RDT
Asst Dir for Project Mgmt, RDT
Liquid Metals Projects Br, RDT:PM
FFTF Project Manager, RDT:PM (3)
Asst Dir for Reactor Engrg, RDT
Control Mechanisms Br, RDT:RE
Core Design Br, RDT:RE (2)
Fuel Engineering Br, RDT:RE
Fuel Handling Br, RDT:RE
Reactor Vessels Br, RDT:RE
Asst Dir for Reactor Tech, RDT
Coolant Chemistry Br, RDT:RT
Fuel Recycle Br, RDT:RT
Fuels & Materials Br, RDT:RT
Reactor Physics Br, RDT:RE
Special Technology Br, RDT:RT
Asst Dir for Engrg Standards, RDT
EBR-II Project Manager, RDT:PM

215 AEC Division of Technical Information Extension

1 AEC Idaho Operations Office
Nuclear Technology Division

C. W. Bills, Director

1 AEC San Francisco Operations Office
Director, Reactor Division

No. of Copies	
4	AEC Site Representatives Argonne National Laboratory Atomics International General Electric Co. Westinghouse Electric Corporation
3	Argonne National Laboratory R. A. Jaross LMFBR Program Office N. J. Swanson
1	Atomic Power Development Assoc. Document Librarian
5	Atomics International FFTF Program Office
2	Babcock & Wilcox Co. Atomic Energy Division S. H. Esleeck G. B. Garton
1	Bechtel Corporation J. J. Teachnor
1	BNW Representative R. M. Fleishman (ZPPR)
1	Combustion Engineering 1000 MWe Follow-On Study W. P. Staker, Project Manager
1	Combustion Engineering 911 West Main Street Chattanooga, Tennessee 37401 Mrs. Nell Holder, Librarian
5	General Electric Company Advanced Products Operation Karl Cohen (3) Nuclear Systems Programs D. H. Ahmann (2)

No. of Copies	
2	Gulf General Atomic Inc. General Atomic Division D. Coburn
1	Idaho Nuclear Corporation J. A. Buckham
1	Liquid Metal Engineering Center
2	Liquid Metal Information Center A. E. Miller
1	Oak Ridge National Laboratory W. O. Harms
1	Stanford University Nuclear Division Division of Mechanical Engrg R. Sher
1	United Nuclear Corporation Research and Engineering Center R. F. DeAngelis
15	Westinghouse Electric Corporation Atomic Power Division Advanced Reactor Systems D. C. Spencer

ONSITE-HANFORD

1	AEC Chicago Patent Group R. K. Sharp
3	RDT Assistant Director for Pacific Northwest Laboratories T. A. Nemzek
2	AEC Richland Operations Office J. M. Shivley
1	Battelle Memorial Institute, Columbus

No. of Copies	
1	Bechtel Corporation
	M. O. Rothwell (Richland)
1	Westinghouse Electric Corporation
	J. D. Herb
68	Battelle-Northwest
	E. R. Astley
	A. L. Bement
	L. R. Besel
	W. L. Chase
	J. C. Cochran
	D. L. Condotta
	J. F. Erben
	E. A. Evans
	G. L. Fox
	P. L. Hofmann
	R. J. Jackson (15)
	M. T. Jakub
	D. C. Kolesar
	F. J. Leitz
	H. E. Little
	W. W. Little (5)
	D. E. Mahagin
	W. B. McDonald
	J. S. McMahon
	I. L. Metcalf (2)
	R. A. Moen
	C. A. Munro (2)
	A. Padilla, Jr.
	J. M. Seehuus
	R. J. Squires
	G. R. Waymire (5)
	J. H. Westsik
	C. L. Wheeler (5)
	B. Wolfe
	Legal-703 Bldg.
	Legal-ROB, 221-A
	BNW-Technical Information (5)
	BNW-Technical Publication (3)
	FFTF File (703) (10)
	FFTF TPO (703)